UCRL-16662

University of California

Ernest O. Lawrence Radiation Laboratory

WORK FUNCTIONS OF MONOCRYSTALLINE AND POLYCRYSTALLINE RHENIUM

TWO-WEEK LOAN COPY

This is a Library Circulating Copy which may be borrowed for two weeks. For a personal retention copy, call Tech. Info. Division, Ext. 5545

Berkeley, California

UCRL-16662 c.2

DISCLAIMER

This document was prepared as an account of work sponsored by the United States Government. While this document is believed to contain correct information, neither the United States Government nor any agency thereof, nor the Regents of the University of California, nor any of their employees, makes any warranty, express or implied, or assumes any legal responsibility for the accuracy, completeness, or usefulness of any information, apparatus, product, or process disclosed, or represents that its use would not infringe privately owned rights. Reference herein to any specific commercial product, process, or service by its trade name, trademark, manufacturer, or otherwise, does not necessarily constitute or imply its endorsement, recommendation, or favoring by the United States Government or any agency thereof, or the Regents of the University of California. The views and opinions of authors expressed herein do not necessarily state or reflect those of the United States Government or any agency thereof or the Regents of the University of California.

UCRL-16662

UNIVERSITY OF CALIFORNIA

Lawrence Radiation Laboratory
Berkeley, California

AEC Contract No. W-7405-eng-48

WORK FUNCTIONS OF MONOCRYSTALLINE AND POLYCRYSTALLINE RHENIUM

Ronald Wichner

(Ph.D. Thesis)

August 1966

TABLE OF CONTENTS

ABSTRACT

I. INTRODUCTION 1

II. THEORY OF THERMIONIC EMISSION 4

A. Review of Thermionic Emission 4

B. Variation of Φ with Crystallographic Orientation 9

III. THE EXPERIMENTAL PROBLEM 17

A. Diode Design 17

B. Emitter Fabrication 21

1. Surface Preparation 21

2. Brazing Studies 21

C. Description of Vacuum System 28

IV. PROCEDURE 30

A. Calibration and Testing 30

B. Experimental Runs 31

V. DISCUSSION OF RESULTS 34

A. I-V and Schottky Plots 34

B. Richardson Plots 47

C. Shelton Plots 52

VI. CONCLUSIONS 55

ACKNOWLEDGEMENTS 56

NOMENCLATURE 57

APPENDIX A.

Electropolishing Solutions 58

APPENDIX B.

Chemical Analysis and Laue X-Ray Pictures of Rhenium 60

APPENDIX C.

The Two-Patch Current-Voltage Characteristic 65

APPENDIX D.

Data Reduction Programs and Error Analysis 69

REFERENCES 100

FIGURE CAPTIONS 103

WORK FUNCTIONS OF MONOCRYSTALLINE AND POLYCRYSTALLINE RHENIUM

Ronald Wichner

Inorganic Materials Research Division, Lawrence Radiation Laboratory,
and, Department of Nuclear Engineering, College of Engineering,
University of California, Berkeley, California

July 1966

ABSTRACT

The bare work functions of polycrystalline rhenium and of the $(10\bar{1}0)$, $(10\bar{1}1)$ and (0001) orientations have been determined for planar emitters, in vacuum, at pressures of 2×10^{-10} to 7×10^{-9} Torr and in the temperature range, 1415°C - 2021°C. Electron emission currents were obtained in a thermionic diode as a function of applied voltage, at a number of temperatures. The work functions were determined by means of the Richardson plot and also deduced from the position of the knee in the current-voltage characteristic. The work function, Φ, and Richardson "A" value, A_r, were found to be as follows:

$$\Phi_{poly} = 4.93 \pm .02 \text{ ev}, \quad A_{r_{poly}} = 74 \pm 21 \text{ amps/cm}^{2\circ}\text{K}^2;$$

$$\Phi_{(10\bar{1}1)} = 5.15 \pm .02 \text{ ev}, \quad A_{r_{(10\bar{1}0)}} = 76 \pm 21 \text{ amps/cm}^{2\circ}\text{K}^2;$$

$$\Phi_{(10\bar{1}1)} = 5.37 \pm .03 \text{ ev}, \quad A_{r_{(10\bar{1}1)}} = 119 \pm 40 \text{ amps/cm}^{2\circ}\text{K}^2;$$

$$\Phi_{(0001)} = 5.59 \pm .05 \text{ ev}, \quad A_{r_{(0001)}} = 199 \pm 49 \text{ amps/cm}^{2\circ}\text{K}^2.$$

A guarded, single-crystal copper collector was employed in a plane geometry configuration in order to minimize edge and other non-uniform effects.

A method was also developed for brazing the emitter buttons to tantalum support cups, using niobium as the high temperature braze material.

I. INTRODUCTION

The field of thermionic energy conversion has received a considerable amount of interest in recent years. The thermionic diode is one of the more promising energy conversion devices by which thermal energy can be converted directly to electrical energy with resaonably high efficiency, reliability and specific power. Thermionic energy converters have been designed for use with various heat sources; nuclear, solar, isotope and chemical,[1,2] and thus appear to be a versatile means for direct conversion of thermal to electrical energy.

Basically, a thermionic diode consists of a hot emitter electrode (typically 1400-2200°K) and a cooler collector electrode. Some of the electrons in the emitter with sufficient thermal energy to overcome the work function barrier, Φ, will escape from the emitter, drift across the inter-electrode gap and fall into the collector, which has a work function Φ_c. If all of the emitted electrons are collected, then we can speak of a saturated current density, J_s. Application of Fermi statistics to electron emission from the emitter surface yields the basic Richardson equation, $J_s = AT^2 \exp\{-\frac{e\Phi'}{kT}\}$.[3]

The most significant property of the emitter which is important to electron emission is its so-called "true" work function (Φ').[4] This is defined as the difference between the energy of an electron which is just capable of being emitted from the metal into field-free space and the energy of an electron at the Fermi level.

Typically, output voltages, electrical power densities and efficiencies of actual converters are 0.2 to 0.4 volt, 1 to 2 watts/cm^2 and 4 to 8%, respectively, at emitter temperatures of 1500°K; and 0.5 to 1.0 volt, 5 to 20 watts/cm^2 and 10 to 19%, respectively, at 2000°K.[1]

These values represent typical performances of thermionic diodes which have had cesium vapor added. The cesium performs two functions. By means of its ionization, it neutralizes the space charge which would be brought about by a high current density of electrons. In addition, it serves to lower the work function of the emitter, which increases the electron emission, and lowers the collector work function, which increases the voltage output. Most of the present work in thermionics deals with cesiated thermionic converters, as they appear to be the most promising high power and high efficiency devices.

Rasor[5] predicted, and later experiments by Gust[6] at Lawrence Radiation Laboratory and by Kitrilakis, et al.[7] at TEECO have shown, that rhenium emitters above 1500°C in a cesium diode are superior to emitters of the other refractory metals. That is, at a given temperature, higher power density is obtained with rhenium emitters than with other emitters or conversely, for a given power density of interest, rhenium emitters can operate 100 or 200°C lower.

This present work deals with the determination of the bare work function of polycrystalline rhenium and the work function of the (0001), $(10\bar{1}0)$, and $(10\bar{1}1)$ orientations. These single crystal orientations were selected because high work functions were expected on theoretical grounds[8,9] and were inferred from field emission experiments.[10]

It is possible that methods for producing oriented surfaces of Re, similar to those for Mo[11] and W[12,13] will be developed so that full advantage of these high work functions will be realized in practical applications.

Chapter II reviews the theory of thermionic emission. Chapters III and IV discuss the design of the experiment and the experimental procedure. Chapter V is devoted to a discussion of the results and

Chapter VI presents a summary and conclusion.

The appendices include derivation of equations, electropolishing recipes, the error analysis and Tables and Figures.

II. THEORY OF THERMIONIC EMISSION

A. Review of Thermionic Emission

The basic equation of thermionics is the well-known Richardson equation,

$$J_s = AT^2 \exp\left\{\frac{-e\Phi'}{kT}\right\} \qquad \text{(II.1)}$$

This equation relates the saturated electron current density to the temperature and work function of the emitting surface. In its derivation, the following assumptions are made:

a. the electrons inside the emitter obey Fermi-Dirac statistics and move in a square-well potential,

b. $e\Phi' > kT$, so that the distribution of electrons around energy $e\Phi'$ can be considered to approximate a Maxwell-Boltzmann distribution,

c. the effective mass of the electrons equals the mass of the free electron, and

d. there is negligible reflection of electrons at the surface.

In the derivation, no assumption is made as to whether or not the work function Φ' is temperature-dependent. The temperature dependence of the work function can, to a first approximation, be represented by[3]

$$\Phi' = \Phi''(To) + \alpha(T-To) = \Phi'' + \alpha T; \qquad \text{(II.2)}$$

where Φ'' is the field-dependent work function. Then, we can rewrite Eq. (II.1) as,

$$J_s = A \exp\left\{\frac{-e\alpha}{k}\right\}T^2 \exp\left\{\frac{-e\Phi''}{kT}\right\} = A_r T^2 \exp\left\{\frac{-e\Phi''}{kT}\right\} \qquad \text{(II.3)}$$

If an accelerating field, F, exists near the surface of the emitter, the work function is lowered by an amount, $\frac{e}{kT}\left(\frac{eF}{\pi\epsilon_o}\right)^{1/2}$. This lowering of the work function barrier is known as the Schottky effect.[14]

Thus, in the presence of an electric field, the saturated current density equation, Ed. (II.3) becomes

$$J_s = A_r T^2 \exp\left\{\frac{e}{kT}\left(-\Phi + \sqrt{\frac{eF}{\pi\epsilon_o}}\right)\right\}$$

$$= J_{so} \exp\left\{\frac{e}{kT}\left(\frac{eF}{\pi\epsilon_o}\right)^{1/2}\right\} \qquad \text{(II.4)}$$

where the field-free saturated current density, J_{so}, and field-free work function, Φ, are defined by

$$J_{so} = A_r T^2 \exp \frac{-e\Phi}{kT} \qquad \text{(II.5)}$$

We see from Eq. (II.4) that if we plot $\ell n J_s$ vs the square root of the applied field, F, we should obtain a straight line whose intercept is J_{so}. This is the "Schottky Plot".

Then, by plotting $\ell n J_{so}/T^2$ vs 1/T, we can obtain from this plot (the Richardson plot) a slope proportional to the work function Φ and an intercept equal to A_r, the Richardson "A" value. If the assumption that α, the temperature dependence of Φ', is small and Eq. (II.2) is valid, then the work function obtained from the Richardson plot is the so-called "true work function". In addition, A_r should equal the theoretical value of A, 120.4 amps/(cm^2-$°K^2$), times $\exp\left\{\frac{-e\alpha}{k}\right\}$, from which α can be deduced.

At this point, it is useful to introduce the concept of the motive diagram. Figure II.1a represents the ideal log current-voltage curve

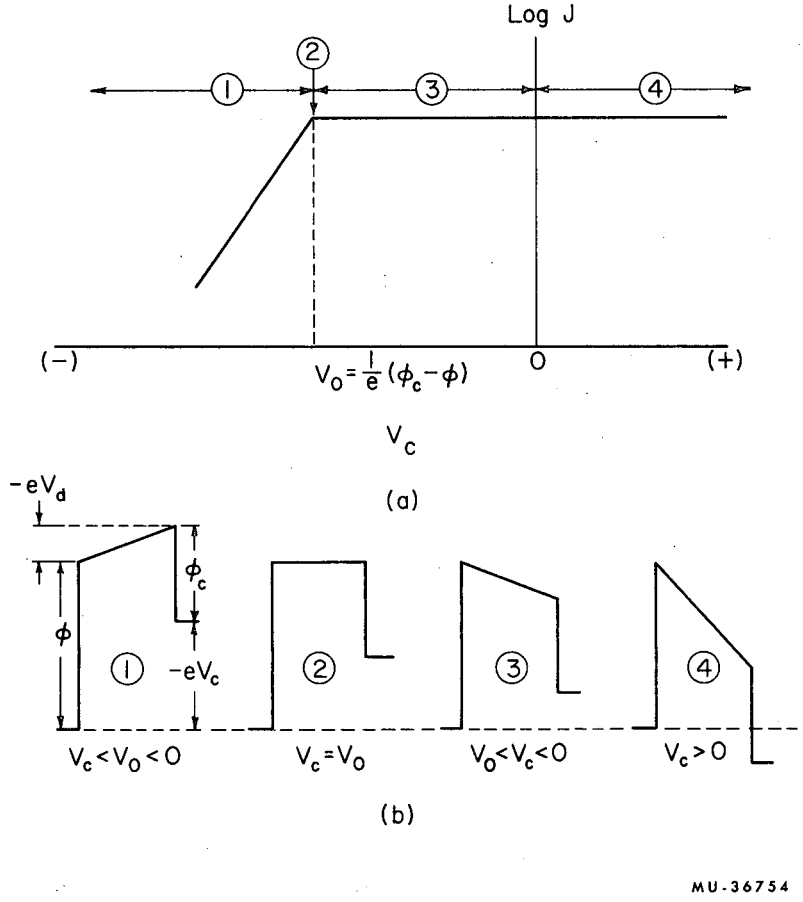
Log J
1
2
3
4
(−)
$V_0 = \frac{1}{e}(\phi_c - \phi)$
0
(+)
V_c
(a)
$-eV_d$
ϕ_c
ϕ
1
$-eV_c$
2
3
4
$V_c < V_0 < 0$
$V_c = V_0$
$V_0 < V_c < 0$
$V_c > 0$
(b)
MU-36754

Fig. II.1

for a vacuum diode having an emitter work function Φ and a collector work function, Φ_c, such that $\Phi' > \Phi_c$.

Region 1 represents the "retarded" region, where the emission current density reaching the collector is less than the saturated emission current density. Figure II.1b shows the motive diagram corresponding to region 1. This diagram depicts the potential that an electron sees in going from the emitter across the diode gap into the collector and through an external circuit back to the emitter. If we consider an electron with just sufficient energy to overcome both the work function barrier, Φ, and the additional decelerating potential, $-eV_d$, it will reach the collector and fall in, giving up an energy, Φ_c. It then has an energy equal to $-eV$ available for external work. In this region the current density is given by,

$$J = J_{so} \exp\left\{\frac{e}{kT}(V - V_o)\right\} \qquad \text{(II.6)}$$

where from region 2, the "knee" of the log J-V curve, we can see that

$$eV_o = \Phi_c - \Phi' \qquad \text{(II.7)}$$

In the motive diagrams corresponding to the saturated regions 3 and 4, we can see that, neglecting the Schottky effect, no additional current is obtained by increasing V, since in order to be emitted, electrons must still have an energy greater than Φ.

The work function of the emitter can also be determined from the value of V_o, the knee. From Eq. (II.7), we see that, in region 1, where $(\Phi_c - eV) > \Phi'$,

$$J = AT^2 \exp\left\{\frac{\Phi_c - eV}{kT}\right\} . \qquad \text{(II.8)}$$

Therefore a plot of $\ell n\ J/T^2$ vs $1/T$ yields a slope proportional to $(\Phi_c - eV)$, where J is obtained at the same V_c for each temperature. This is the so-called "Shelton Plot".[15]

Since we can obtain a value for $(\Phi_c - eV)$, and we know V, we can find Φ_c. From this, and finding the value of V_o from the log J-V curve we can use Eq. (II.7) to find Φ'.

If the collector temperature is kept constant, then the intercept of the Shelton plot should, in theory, yield an "A" value of 120 amps/cm^2-°K^2, regardless of the temperature dependence of Φ_c. In addition, the temperature calculated from the slopes of the log J-V curves should be the same as the observed value, otherwise the intercept will not yield the theoretical value of A.

B. Variation of Φ With Crystallographic Orientation

To the present time, the prediction of the work function of bare metallic surfaces has been hampered by the complex problem of defining the shape of the potential at the surface. According to Wigner and Berdeen,[16] the work function can be thought of as being composed of two parts, an inner work function, dependent only upon the binding energy of an electron in the metal, and a surface contribution, dependent upon the energy an electron needs to penetrate a dipole double layer at the surface. Wigner and Bardeen derived an expression for the inner work function of metals, based on the assumption that the wave functions of the free conduction electrons were plane waves over much of the unit cell. This theory and its modifications are useful only for the monovalent elements on the left side of the periodic chart, where the inner work function is a major portion of the observed work function.[17] However, for the more complex atoms of the periodic chart, the surface contribution to the work function must be taken into account. Bardeen[18] extended this theory to include the contribution of a generalized surface double layer. Smoluchowski,[8] however, was the first to attempt to calculate the different work functions of specific orientations of a metallic surface. Following the lead of Wigner and Bardeen, he separated the work function into an inner contribution and a surface contribution. For the surface contribution to the work function, he proposed the following model. First, he assumed that the positive charge of each ion core is uniformly distributed over the entire polyhedral volume that each atom has geometrically associated with it. In the interior of the metal, the electron-cloud density is evenly distributed over each atomic polyhedron. If this were the case at the surface, then no dipole layer would

result. However, at the surface, there is a redistribution of the electron cloud, but the positive charge distribution associated with each atom remains essentially uniform. This redistribution of electrons can be described in two parts: 1. The electrons tend to spread out, away from the surface, because of the concentration gradient between the metal and free space. In other words, the electron density cannot change abruptly from the bulk electron density inside the metal to zero just beyond the surface but must do so continuously if the surface is to have a minimum energy. This results in a negative charge away from the surface, and since the electrons had to come from the above polyhedral volume, they leave behind a net positive charge. Thus, a negative dipole layer is formed which has the effect of increasing the barrier for electron emission, i.e., it increases the electron work function.

2. The other effect of the redistribution can be a smoothing out of the electron cloud on the surface. This smoothing comes about from the decrease in energy associated with electrons flowing from the "peaks" into the "valleys" formed by the surface polyhedra. This flow of negative charge tends to leave the tips of the surface polyhedra positive and the increase in electron density in the valleys produces a negative charge. Hence this effect tends to form a positive dipole layer at the surface, i.e., the work function tends to decrease.

Unfortunately, to obtain numerical values, the model proposed by Smoluchowski requires several simplifying assumptions, including the assumption of a linear variation in the density of free electrons near the surface due to spreading, and an assumption of the number of free electrons per atom in the metal.

The dipole moment due to spreading, which increases the work function, increases with increasing packing density of atoms on the surface. On the basis of this consideration, the work function of tungsten should decrease in the order of the (110), (100), (112), (111), (116) orientations. This is confirmed by experiment except for the (112) orientation, whose work function falls between that of the (100) and (111) planes. Smoluchowski has shown that consideration of the change in dipole moment due to smoothing leads to a prediction of the work functions of tungsten in the same order as those experimentally observed.

Stickney[9] has observed that this same order for tungsten is achieved if it is assumed that the work function increases with the number of near neighbors seen by a given atom on the surface. Following this approach, he constructs around a central atom a number of concentric shells containing the neighboring atoms. Table II.1 indicates the number of atoms contained in each shell for a body-centered cubic lattice, e.g., that of tungsten, for the different orientations and the corresponding work functions. Table II.2 indicates a corresponding list of several orientations of rhenium, which is a close-packed hexagonal lattice, listed in order of decreasing near neighbors, and therefore in order of expected decreasing work function. Figure II.2 depicts the rhenium lattice from which the radii of the shells were obtained.

Using this model, the work function of the (0001) orientation should be the highest and the work functions of the $(10\bar{1}0)$ and $(10\bar{1}1)$ should be lower but about equal to one another.

On the basis of the surface density of different orientations obtained from x-ray diffraction measurements,[20] the order of decreasing work functions should be (0001), $(10\bar{1}0)$, and $(10\bar{1}1)$. Table II.3 shows the variation of interplanar distance with orientation. Since the volumetric density in

the crystal is constant, the surface density is directly proportional to the interplanar distance.

This brief analysis is compared with experimental results in Sec. V.

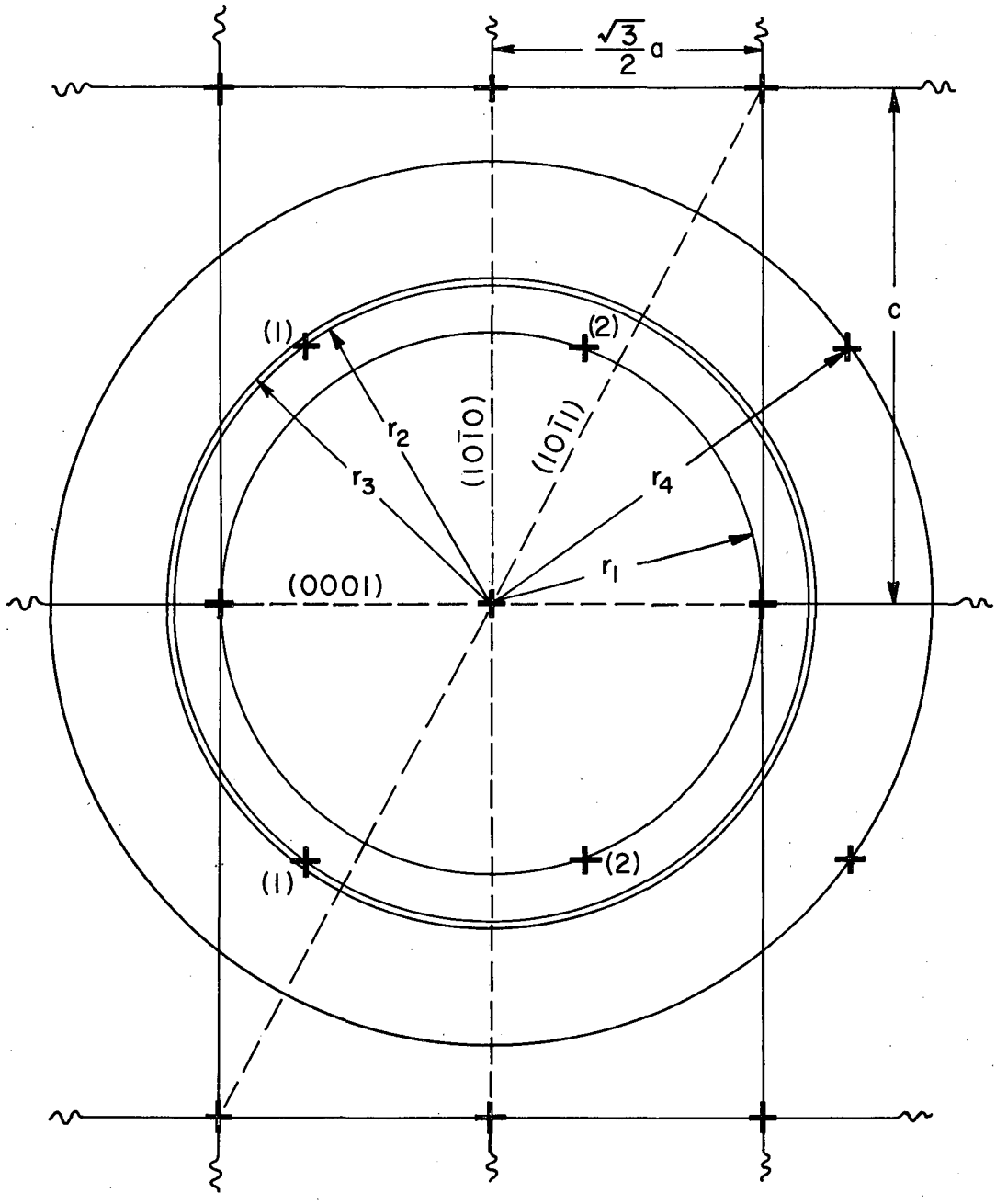

MUB-12045

Fig. II.2

Table II.I

Number of Near Neighbors Associated with a Given Bulk- or Surface-Atom of (BCC) Tungsten[9]

	Number of Atoms in Shell of Radius, r_i				Work function
	r_1	r_2	r_3	r_4	ev
Value of r_i	$a\frac{\sqrt{3}}{2}$	a	$a\sqrt{2}$	$\frac{a}{2}\sqrt{11}$	-
Bulk	8	6	4	8	(4.55)
110 Surface	6	4	3	4	5.24
112 Surface	5	3	3	4	4.65
100 Surface	4	5	4	4	4.52
111 Surface	4	3	3	6	4.38
116 Surface	4	3	3	4	4.29

a = lattice constant of tungsten = 3.165Å

Table II.II

Number of Near Neighbors Associated with a Given Bulk- or Surface-Atom of Rhenium

	Number of Atoms in Shell of Radius, r_i			
	r_1	r_2	r_3	r_4
Value of r_i	$1/2\sqrt{\frac{a^2}{3} + c^2} = 2.36\mathring{A}$	$\sqrt{\frac{a^2}{3} + \frac{c^2}{4}} = 2.69\mathring{A}$	$a = 2.76\mathring{A}$	$\sqrt{\frac{4}{3}a^2 + \frac{c^2}{4}} = 3.89\mathring{A}$
Bulk	4	2	6	2
(0001) Surface	2	1	6	1
$(10\bar{1}0)$ Surface	2	1	4	1
$(10\bar{1}1)$ Surface	2	1	4	1

Table II.III

Variation of Interplanar Distance with Crystallographic Orientation of Rhenium, Listed in Order of Expected Decrease in Work Function

Crystallographic Orientation	Interplanar Distance
(0001)	4.452 Å
$(10\bar{1}0)$	2.388 Å
$(10\bar{1}1)$	2.105 Å

III. THE EXPERIMENTAL PROBLEM

A. Diode Design

The thermionic diode used in these experiments is shown in Figs. III.1 and III.2. In Fig. III.1, all electrical and thermocouple leads are shown, in addition to three vertical quartz heaters (GE-T5) which were used, originally, to bake out the system. However, these heaters have since been removed because the viewing ports became too hot as a result of the absorption of the infra-red radiation. Figure III.2 shows schematically, the design of the diode. The electron gun and emitter support cup were fabricated by Litton Engineering Laboratories (Grass Valley, Calif.). The electron-gun filament was a tungsten coil spot-welded to a Mo center lead and a Mo outer heat shield. Each emitter button (17/32" diameter × 3/16" thick) was brazed with Nb to the Ta support cup, as described in Section III.B. The collector assembly consisted of a single crystal (100) copper collector (.384" diameter) and guard-ring, each brazed to an OFHC copper support, and a cooling plate. The gap between the collector and guard-ring was 5 - 7 mils. It was necessary to insulate the collector, guard-ring and cooling plate electrically, but still provide for sufficient thermal conduction to constant collector and guard-ring temperature. Alumina was first flame-sprayed on the collector support plate to provide insulation between the collector and guard-ring. However, this proved to be unreliable. During some of the preliminary experiments, the insulation broke down at one or two points. Therefore, a piece of electronic-grade mica, approximately 2 mils thick, was added to provide additional insulation. However, this increased the thermal resistance, which decreased the sensitivity of the collector temperature to the cooling-

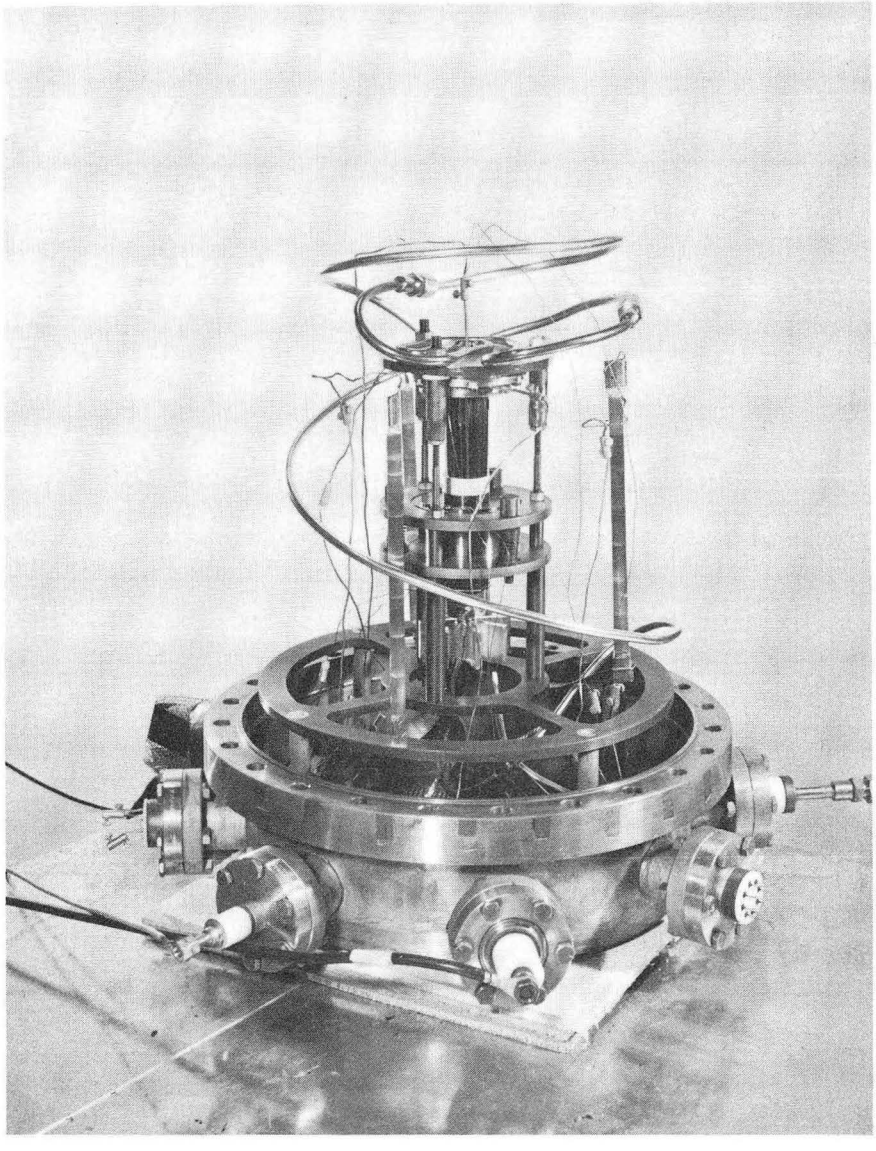

ZN-5731

Fig. III.1

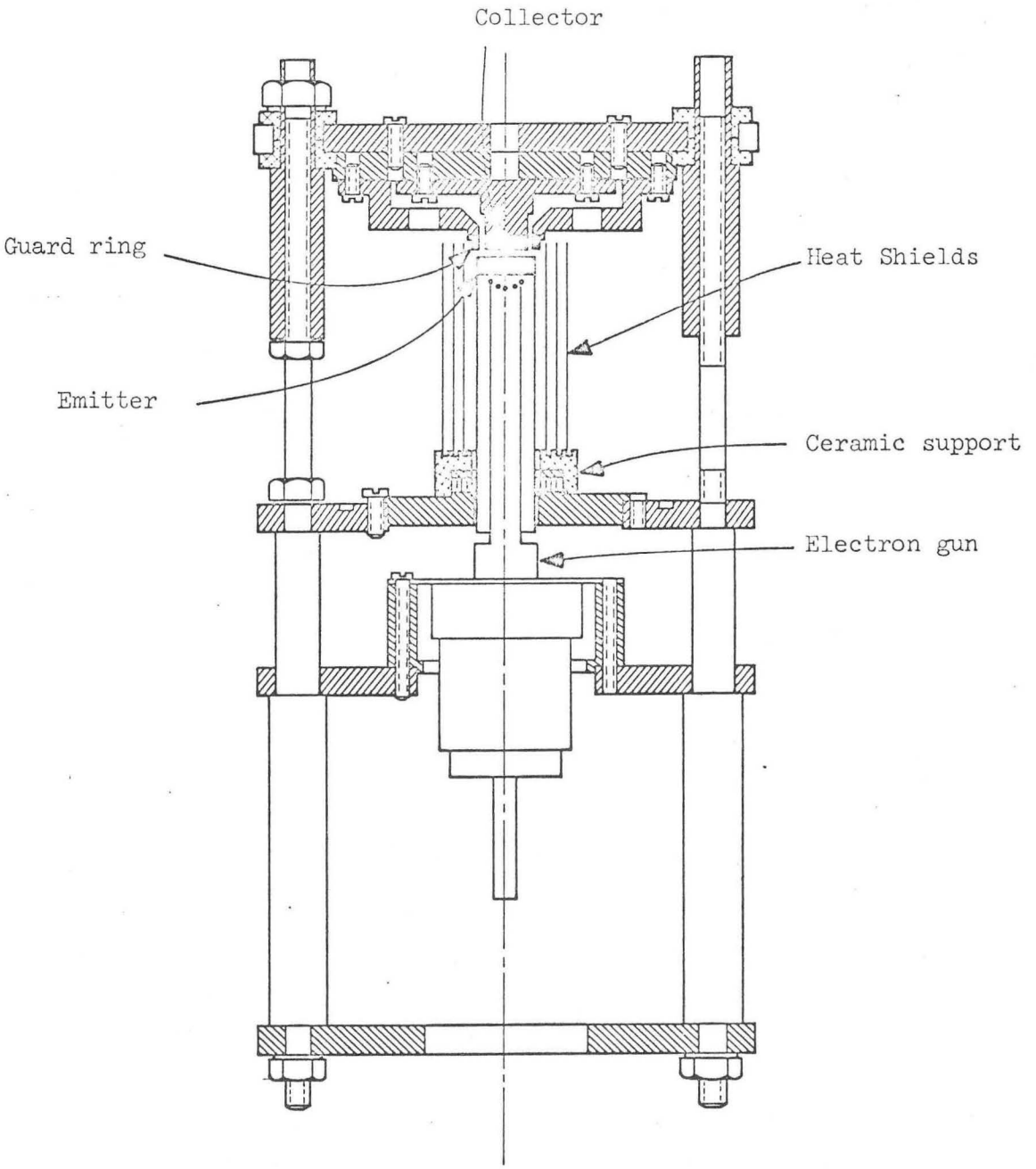

MU-36621

Fig. III.2

B. Emitter Fabrication

1. Surface Preparation

The emitters were cut from the polycrystalline and monocrystalline rods using a "Servomet" spark cutter. The buttons were then planed on the "Servomet" to a finish of approximately 10 microinches (center line average). This was sufficient, in the case of the single crystal emitters, to permit their proper orientation, with the aid of Laue´ back reflection pictures. Once properly oriented to within 2°, they were then planed again, if needed, and brazed to the Ta support cups, as described below.

After being brazed, the emitters were then ground down on 4/0 emery and rough polished with a 1μ diamond suspension in kerosene. It was found that unless heavy pressure was kept on the specimen in the rough polishing stage, pitting of the surface occurred. In addition, attempts at mechanical polishing with anything else but 1μ diamond resulted in pitting of the surface. After the surface of each emitter was mechanically polished to a scratch-free condition, it was electropolished for several seconds in polishing solution number 1 described in Appendix A. Longer periods of electropolishing resulted in pitting of the surface, so a combination of mechanical polishing and electropolishing was employed to obtain a distortion- and pit-free surface.

Laue´ x-ray photographs of each of the orientations and a chemical analysis of the rhenium are presented in Appendix B.

2. Brazing Studies

It was necessary that the bond between the rhenium emitter buttons and tantalum support cups meet the following requirements:

a. the joint must withstand thermal cycling between room temperature and 2200°C,

b. the brazing filler, if any, must have a low vapor pressure, and

c. the melting temperature of the joint must be above 2300°C.

Requirements b and c narrowed the selection of materials to those metals which did not form eutectic or peritectic compositions, with either tantalum or rhenium, at temperatures below 2300°C. In addition, the thermal cycling requirement suggested that it would be wise to avoid the formation of a σ-phase in the region of the joint, since this complex phase has a tendency to be more brittle than simpler phases.

In view of the above, niobium foil was selected for use as the brazing material. Among the metals under consideration, only niobium does not appear to exhibit a σ-phase.[21] There is some disagreement in the literature, however, as Knapton[22] claims the existence of a σ-phase over a narrow range of composition and temperature. In case this phase does exist in the Nb-Re phase diagram, the steps taken below were designed to ensure that none existed in the bond between the emitter button and support cup after the brazing process was completed.

Prior to brazing, Hohlraums, .016" in diameter and .100" deep, were spark-machined into the sides of the emitter buttons. The buttons were then electropolished until all traces of carbon and copper from the spark cutting process were removed. The Nb foil (2mils thick) and the Ta support cups were chemically cleaned with standard[23,24] cleaning solutions.

Figure III.3 is a photograph of the vacuum brazing stand. It is constructed of stainless steel, alumina standoffs and graphite discs, which hold the tantalum heat shields and tantalum support cup. For

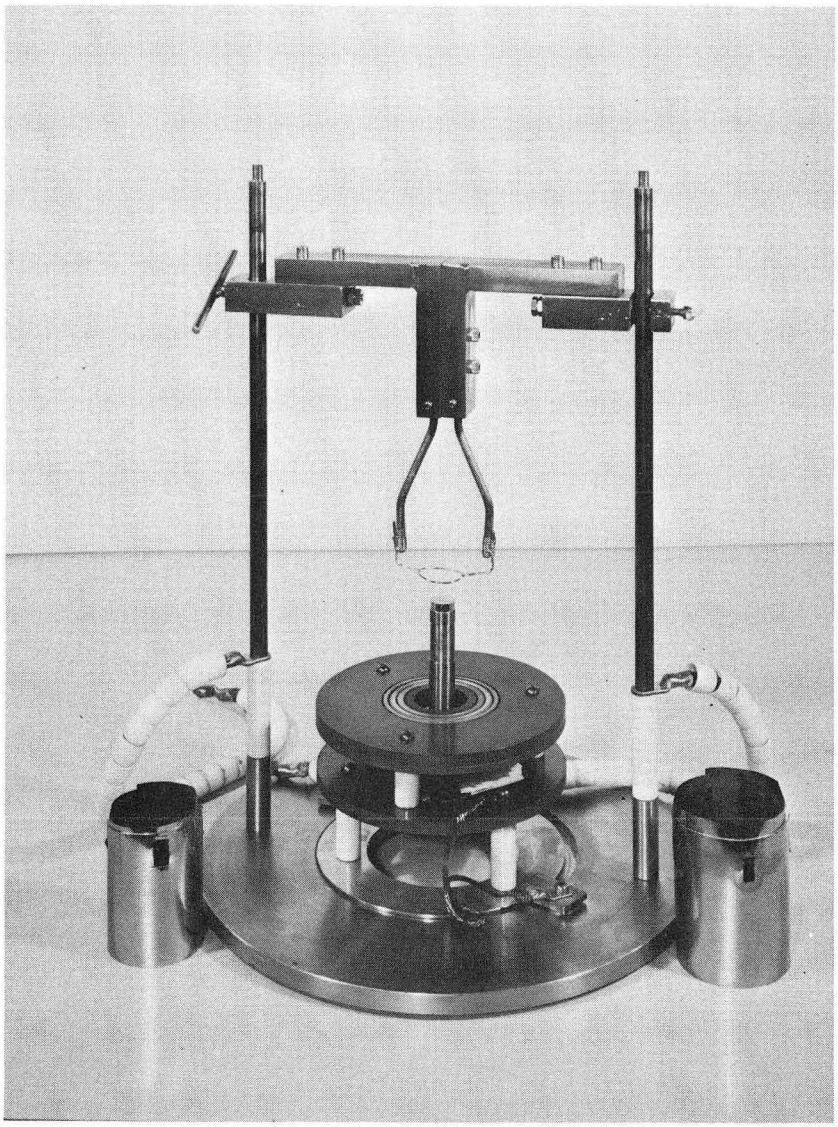

ZN-5730

Fig. III.3

preliminary brazing studies, tantalum discs, approximately 1/8" thick × 1/2" in diameter were brazed to equal size polycrystalline Re discs, using 2 mil niobium as the braze material. The filament consisted of two 35 mil tantalum wires spot-welded together to form a circular filament with two leads. A current of 90 amps was sufficient to heat the filament to approximately 1950°C, observed.

By electron bombardment, the temperature of the Re-Nb-Ta sandwich was increased to the melting point of the niobium. This corresponded to approximately 2470°C (black-body temperature), at an emission current of approximately 600 ma and a potential of 1000 volts. After the Nb was observed to have melted, the temperature was raised to 2530°C for a minute to ensure complete melting of the niobium. The temperature was then lowered at a rate of 75°C per minute to 2200°C, at which point it was held for approximately 5 minutes. Since the σ-phase is not stable at or below this temperature, this was done to ensure that, in the event a σ-phase had formed between the rhenium and niobium, it would decompose into other phases before the rate of the solid-state reactions decreased to a negligible value. The temperature was then decreased at approximately the same rate (75°C/min.) to ambient conditions. A CVC PS-40A vacuum system was used to maintain vacuum conditions during brazing, and the pressure in the system was kept below 5×10^{-5} torr for all brazes.

Figure III.4 shows the results of early attempts at brazing. The niobium used in the early experiments contained approximately 600 ppm of oxygen and nitrogen,[25] which resulted in the formation of voids all along the rhenium-niobium interface. This resulted in mechanically poor joints. In subsequent brazes the niobium was outgassed at 2300°C

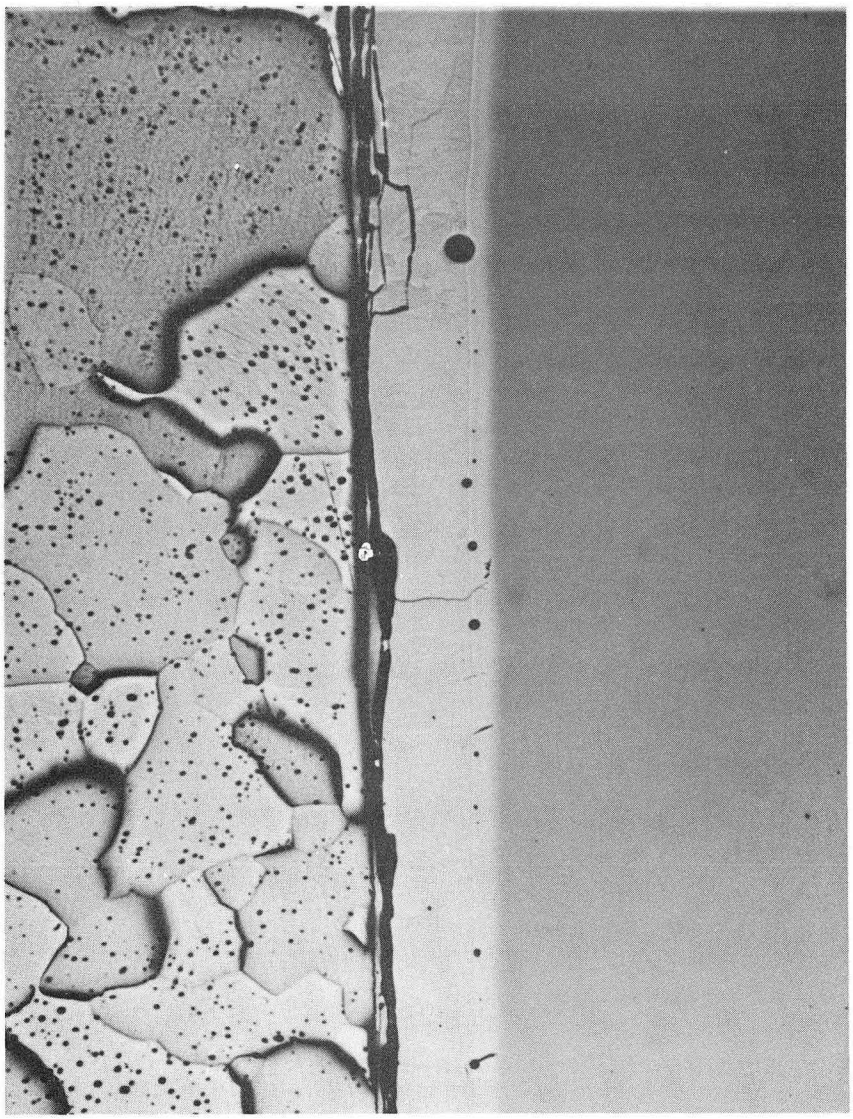

Re Nb Ta

ZN-5732

Fig. III.4

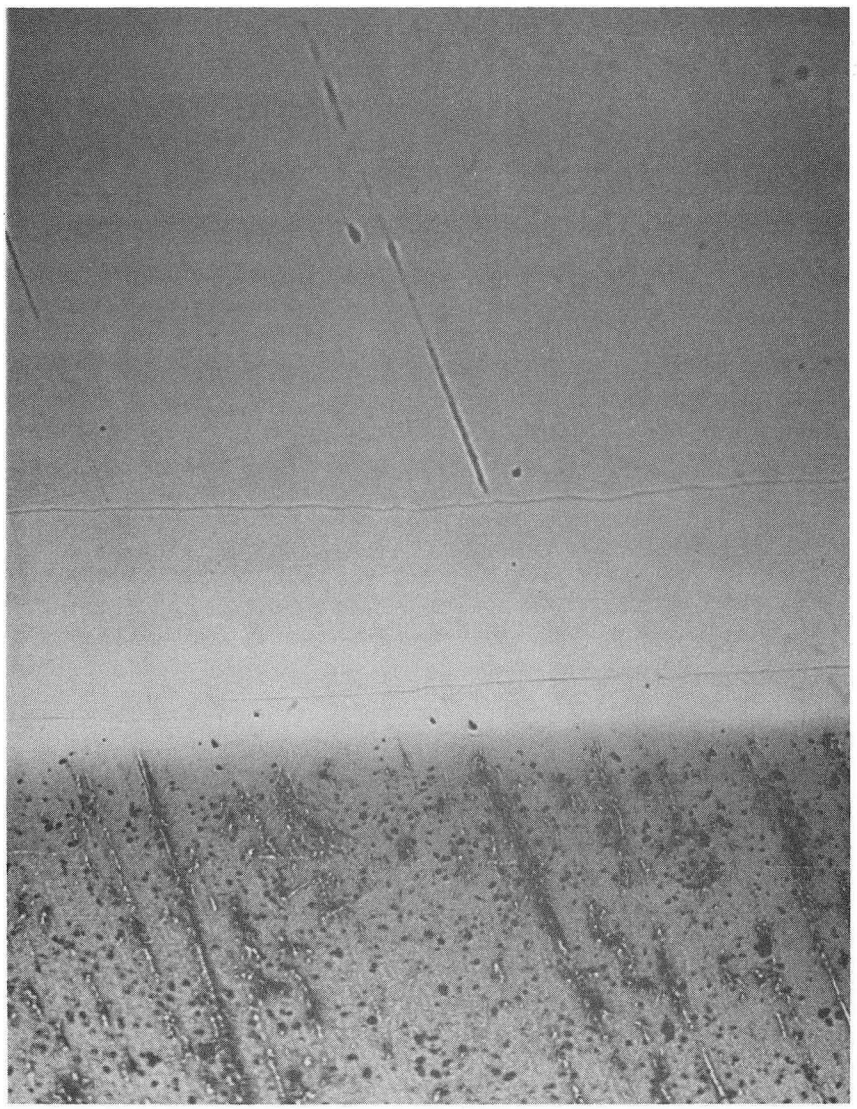

ZN-5736

Fig. III.5

C. Description of Vacuum System

The vacuum system used in the thermionic emission experiments is shown in Fig. III.6. The bell jar was constructed of .065" stainless steel and was 14" high and 14" ID. Eight 1-1/2" feedthroughs were used for all electrical connections to the diode. Two 4" glass viewing ports were used for optical aligning, spacing and temperature measurements. All seals were metal-metal seals. Seals for the 14" and 6" flanges were Al foil seals designed after Batzer[19] and all others were commercial Cu-gasket seals. Pumpdown was accomplished by evacuating the system to approximately 27 inches of mercury by means of the house vacuum line. The sorption pump (Varian "Vac-Sorb") was then used to bring the system pressure to less than 5μ, at which time the ion pump (Ultek, 100 l/sec) was turned on. After the chamber had been baked out, and the pressure was below 10^{-7} torr, the Ti sublimation pump, whose chamber was 10 inches in diameter, was turned on. This pump, whose effective pumping speed was approximately 2500 ℓ/sec, was then used, in conjunction with the ion-pump, to bring the pressure down to the base pressure of $\sim 10^{-10}$ torr.

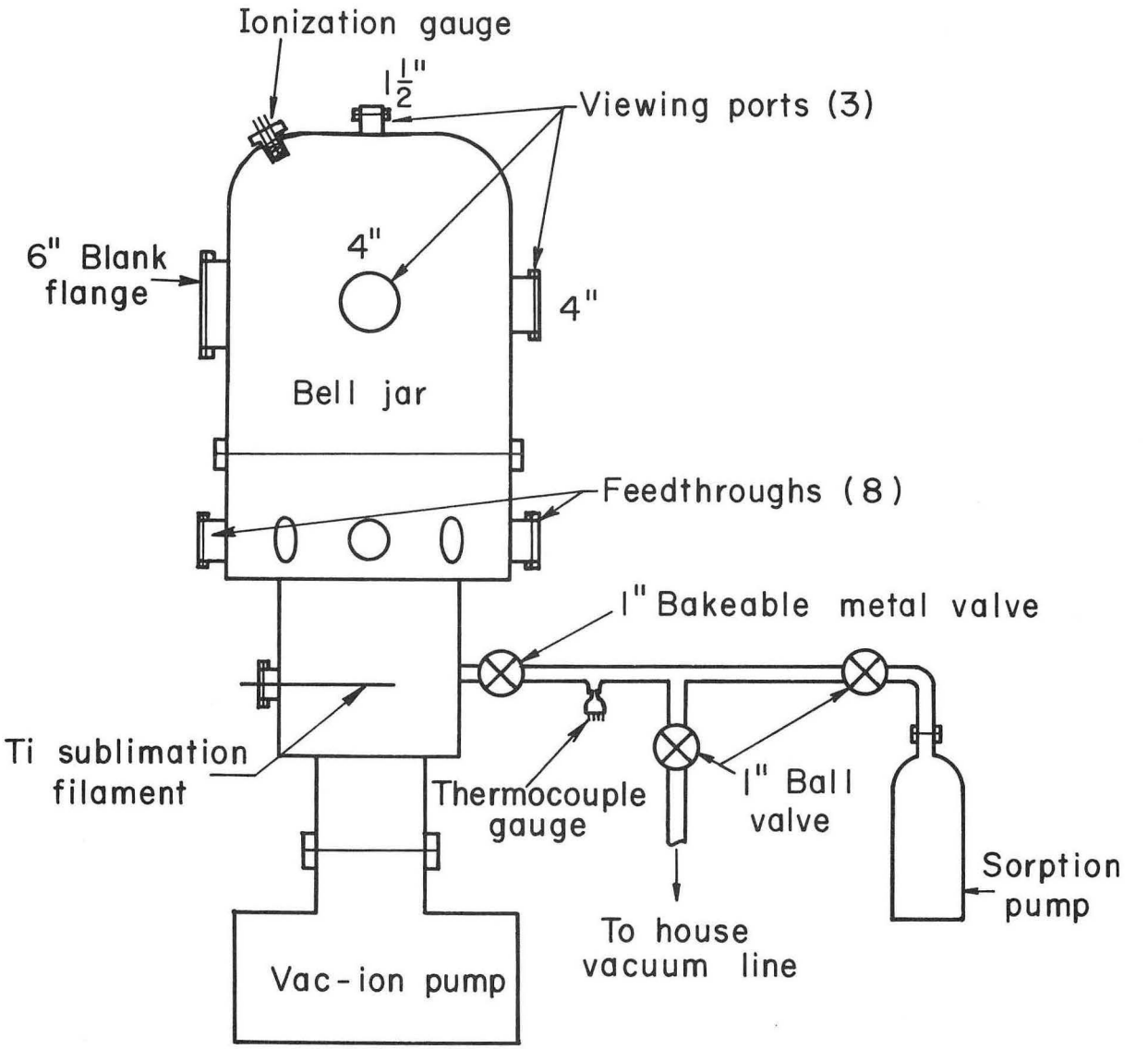

MUB-10039

Fig. III.6

IV. PROCEDURE

A. Calibration and Testing

The gap between the emitter and collector assembly was set to approximately 0.75 mm and adjusted with the aid of a cathetometer so that the emitter and collector were parallel to within ±.01 mm. The gap was set at this value to allow for thermal expansion of the emitter support cup, since there were no means by which the diode spacing could be adjusted during the experiment. The spacing varied between 0.3 mm and 0.05 mm when the diode was hot.

After all electrical leads and thermocouples were connected, the vacuum chamber was sealed and the system brought down to approximately 10^{-6} torr. At this point, two 6-foot heating tapes were used to bake out the chamber at 400°C. The power to the heating tapes was increased slowly so that at no time was the pressure allowed to go above 5×10^{-5} torr, for fear the ion pump would shut itself off. After baking the chamber at 400°C for about 24 hours, the temperature was slowly lowered to room temperature. The emitter was then heated up to 10°C above its maximum temperature, in all cases close to 2000°C, and kept there for at least 6 hours. This was done to outgas those parts of the diode which would otherwise outgas during the runs. In this manner, and with the aid of the Ti sublimation pump, the pressure in the chamber was kept between 2×10^{-10} and 7×10^{-10} torr for all runs below 1800°C and between 7×10^{-10} and 7×10^{-9} torr for all runs at temperatures above this value. The entire bakeout process normally took a period of approximately 96 hours.

Approximately 8 hours before each set of runs, all of the instrumentation was turned on in order to minimize drift of the electronics.

The instrumentation amplifiers were zeroed just prior to each set of runs. Two sets of runs were taken for each emitter, on successive days.

A Micro-Optical pyrometer was used to determine the black-body temperature of the emitters to within ±5°C. This pyrometer was calibrated with a GE notched-tungsten filament calibration lamp. Figure IV.1 shows the calibration curve used, and includes a correction for absorption in the glass viewing port through which the emitter temperature was taken.

B. Experimental Runs

At each temperature for which a current-voltage characteristic was taken, the following was recorded, before and after: Emitter temperature, collector temperature, emitter-collector gap, pressure, electron gun current and voltage. In addition the guard ring temperature was measured every 3 or 4 runs. Although the emitter temperature stabilized in less than 5 minutes, it was necessary to wait approximately 15 minutes for the collector temperature to stabilize. The collector temperature was maintained to 150°C ±25°C over the entire temperature range of the emitter by adjusting the coolant water flow rate.

Data were taken first, at maximum emitter temperature, and then at roughly equal intervals down to the minimum temperature. The emitter was then raised again to several intermediate temperatures and additional data were taken.

The following day, a similar series of data was taken, and the emitter was finally flashed to its maximum temperature from a relatively low temperature and allowed to cool rapidly. Typically, the temperature would drop 400°C in 20 seconds. When the temperature stabilized again, about 3 minutes after flashing, another set of data was taken. This was done

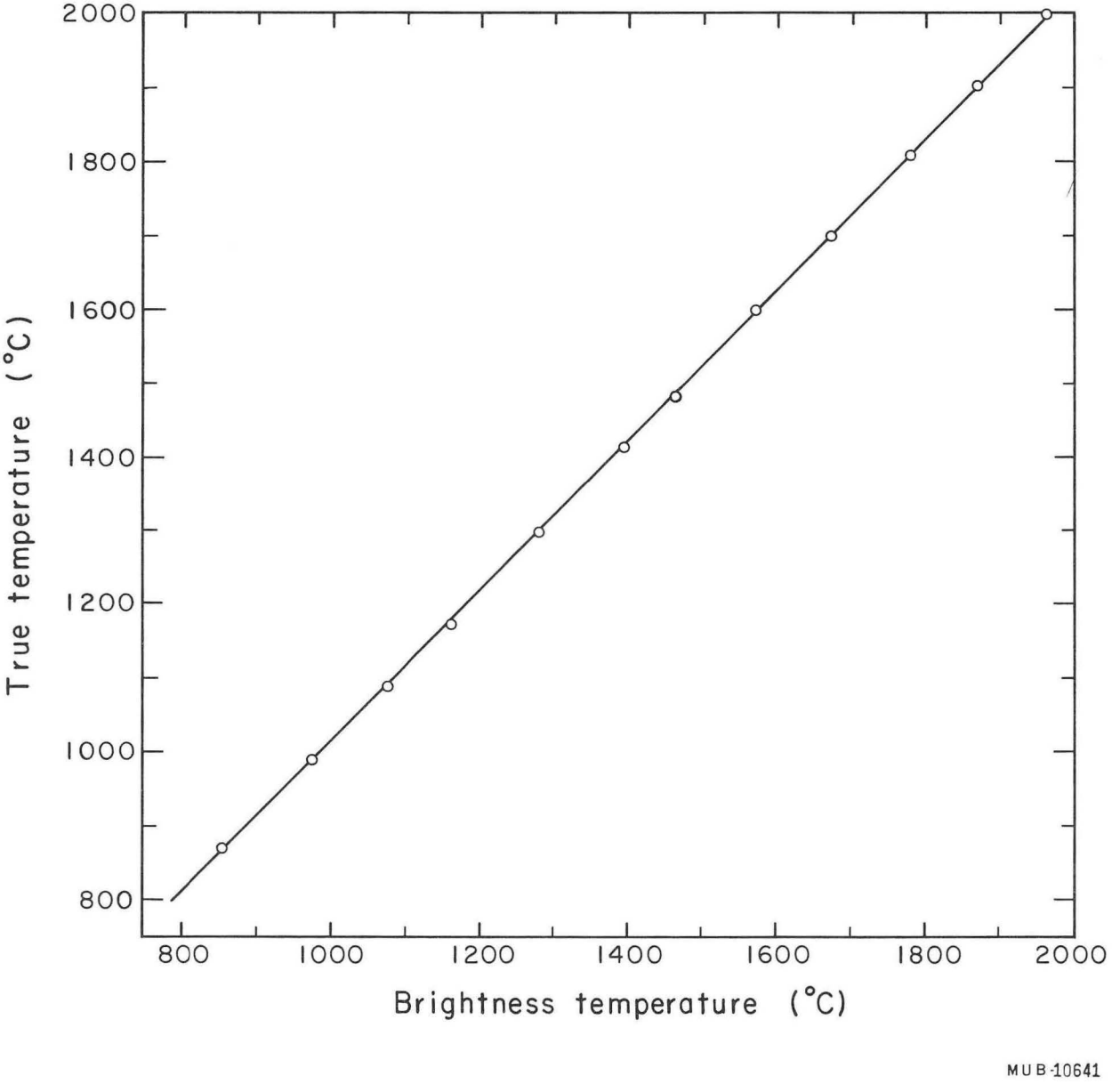
2000
1800
1600
1400
1200
1000
800
True temperature (°C)
800
1000
1200
1400
1600
1800
2000
Brightness temperature (°C)
MUB-10641

Fig. IV.1

to see whether any changes in work function had occurred because of adsorption of gases on the surface of the emitter. (The results indicate no such changes.)

V. DISCUSSION OF RESULTS

A. I-V and Schottky Plots

A sample ℓn J-V curve is shown in Fig. V.1. Figure V.2 shows an expanded view of the retarded region before it was corrected for resistive leakage current. These figures are typical of all of the ℓn J-V curves obtained in these experiments. At low current densities the curve deviates from the straight line because of resistive leakage in the diode. Figure V.3 shows the current-voltage characteristic on rectilinear coordinates. The linear portion of the curve yields an estimate of the resistive leakage in the diode. This resistive current, which is a function of the applied voltage between the emitter and collector, was subtracted from the data. Figure V.4 shows the corrected ℓn J-V curve. Each of the ℓn J-V curves obtained in these experiments were corrected for resistive leakage. The leakage resistance in the diode varied from approximately 4.5×10^{10} ohms at the beginning of the experiments to 1.1×10^{8} ohms near the end. This resistance was very sensitive to changes in the collector temperature, which implies that the mica insulation in the collector assembly was very sensitive to expansion or contraction effects.

At the knee of the ℓn J-V curve, where one would expect a sharp break in the ideal situation, it was observed that width of this transition region varied with emitter temperature, diode spacing and also with emitter orientation.

The broadening of the knee is a result of space charge effects and inhomogeneities at the emitter or collector surfaces. Edge effects were minimized by means of the guarded geometry. The width of the knee varied

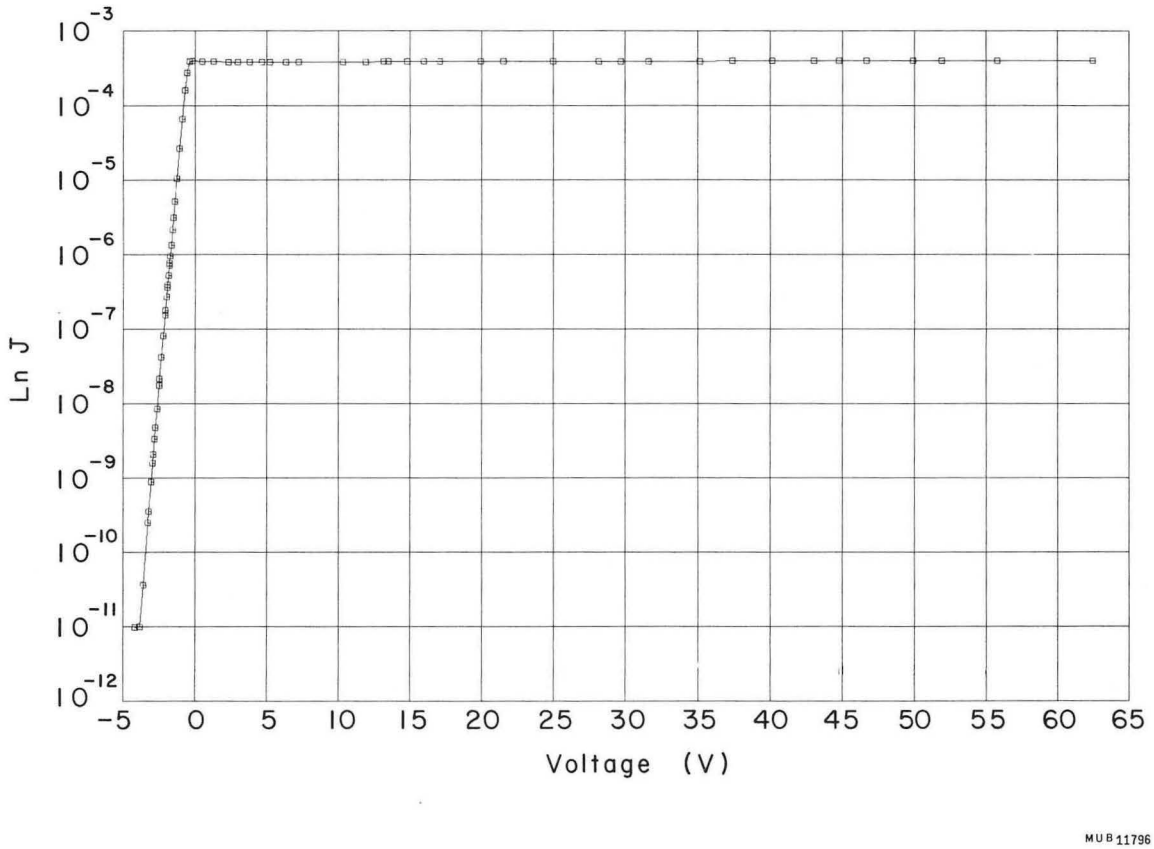
10^-3
10^-4
10^-5
10^-6
10^-7
10^-8
10^-9
10^-10
10^-11
10^-12
Ln J
-5
0
5
10
15
20
25
30
35
40
45
50
55
60
65
Voltage (V)
MUB 11796

Fig. V.1

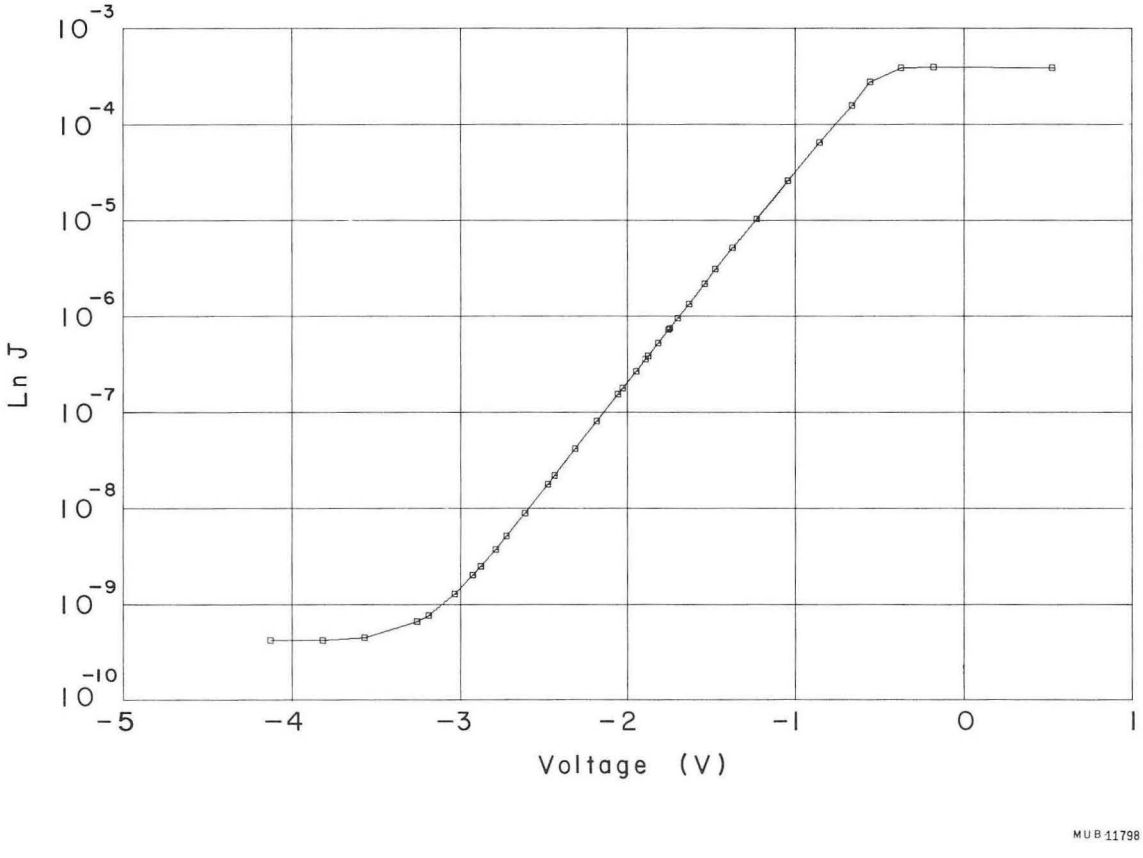
10^-3
10^-4
10^-5
10^-6
10^-7
10^-8
10^-9
10^-10
Ln J
-5
-4
-3
-2
-1
0
1
Voltage (V)
MUB 11798

Fig. V.2

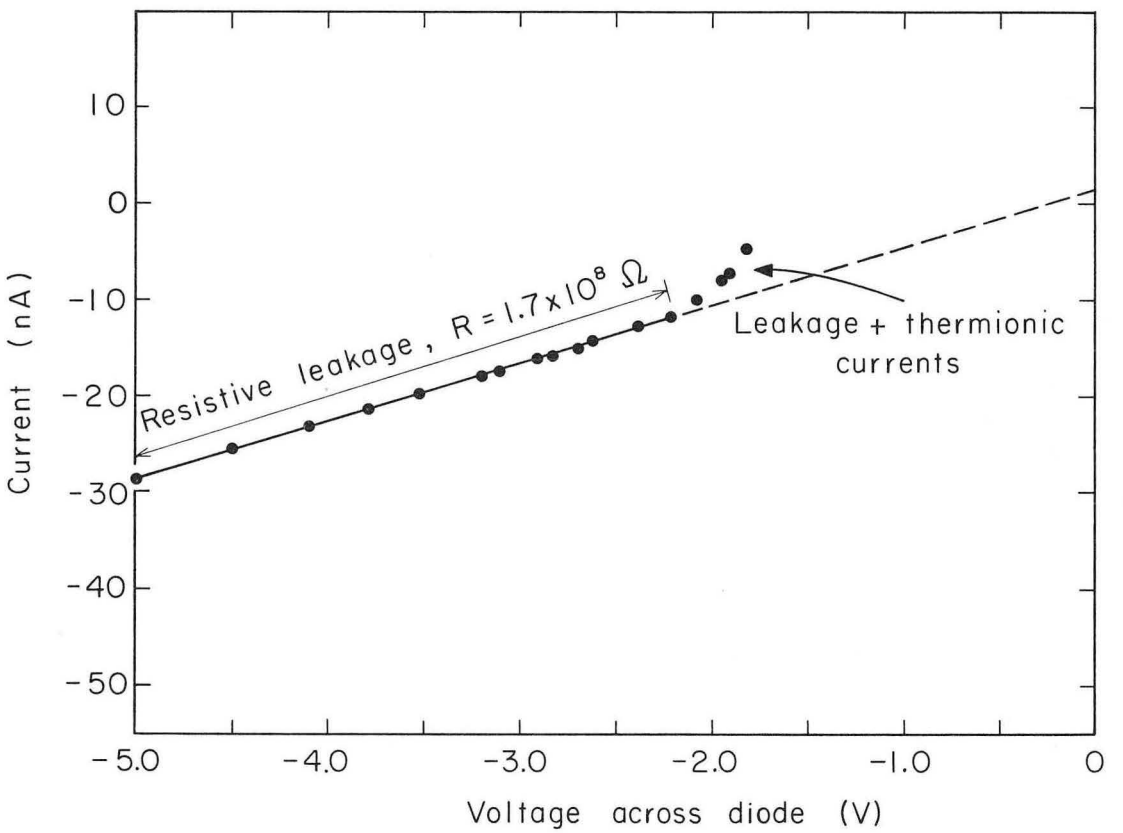

MUB-12046

Fig. V.3

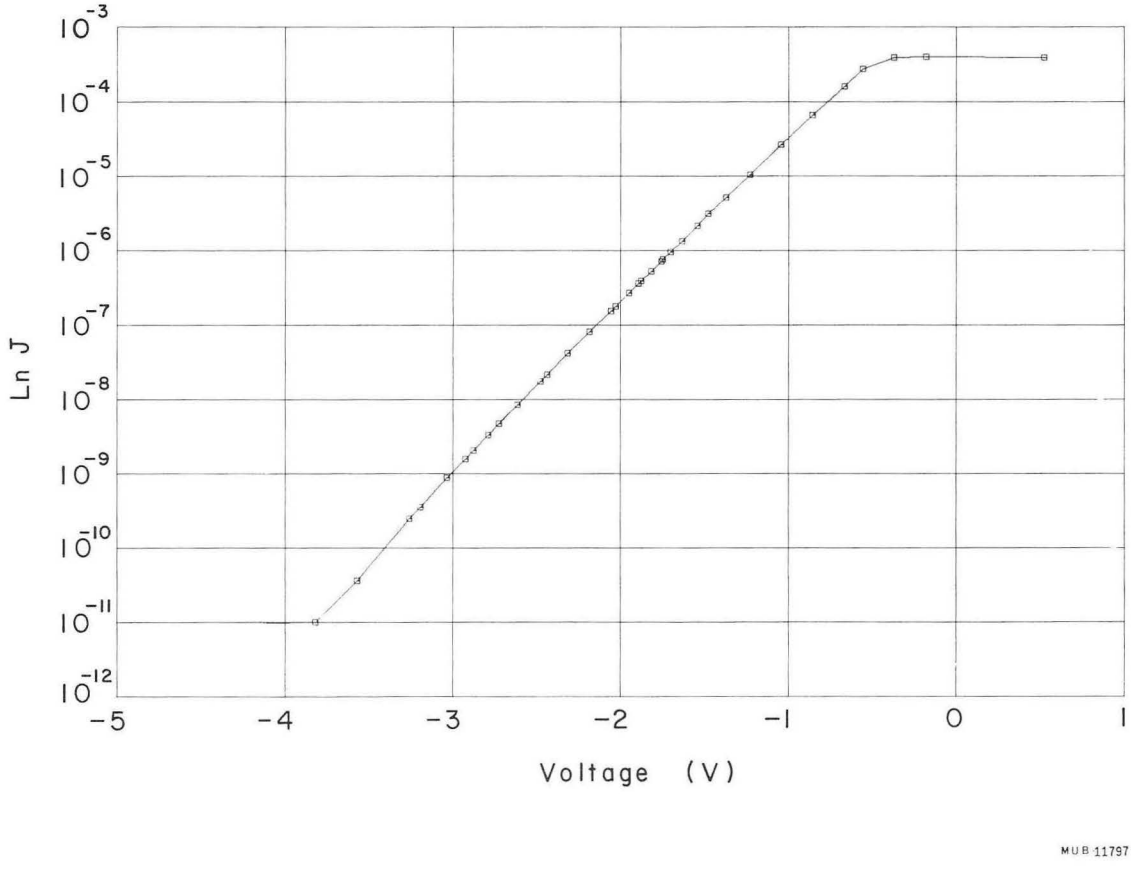
10^-3
10^-4
10^-5
10^-6
10^-7
10^-8
10^-9
10^-10
10^-11
10^-12
Ln J
-5
-4
-3
-2
-1
0
1
Voltage (V)
MUB 11797

Fig. V.4

from more than 0.7 volts at high current densities with the polycrystalline emitter to less than 0.1 volts at low current desnities with the $(10\bar{1}1)$ emitters. The knee in the $\ln$ J-V curves of the (0001) consisted of two relatively sharp breaks at low current densities, as shown in Fig. V.5. This is probably a result of a two-patch emitter surface, as discussed below. The knee of the $(10\bar{1}0)$ emitter was also not as narrow as would be expected. It is probably a result of surface inhomogeneities, as shown in Fig. V.6, where the surface of the $(10\bar{1}0)$ emitter, viewed at 400× magnification after the experiment, appears to have undergone some rearrangement. This rearrangement results in a barely perceptible broadening of the spots of a Laue x-ray picture, so no conclusion as to its structure can be made. This surface structure, plus the comments below lead us to the conclusion that the $(10\bar{1}0)$ emitter may not, in fact, have had a surface arrangement of atoms completely representative of the $(10\bar{1}0)$ orientation.

The Schottky plots were found to be linear, as expected, above approximately 10 volts up to the maximum applied voltage, 65 volts. Below 10 volts, the curves deviated from a straight line as a result of space charge, surface reflection of electrons, or minor misalignment of the emitter and collector. However, the temperature of the emitter, as calculated from the slope of the Schottky plot, was typically within 10% of the observed temperature. This indicates that in the linear region, the applied field overshadowed the above-mentioned effects and the application of Schottky theory is valid. A typical Schottky Plot is presented in Fig. V.7.

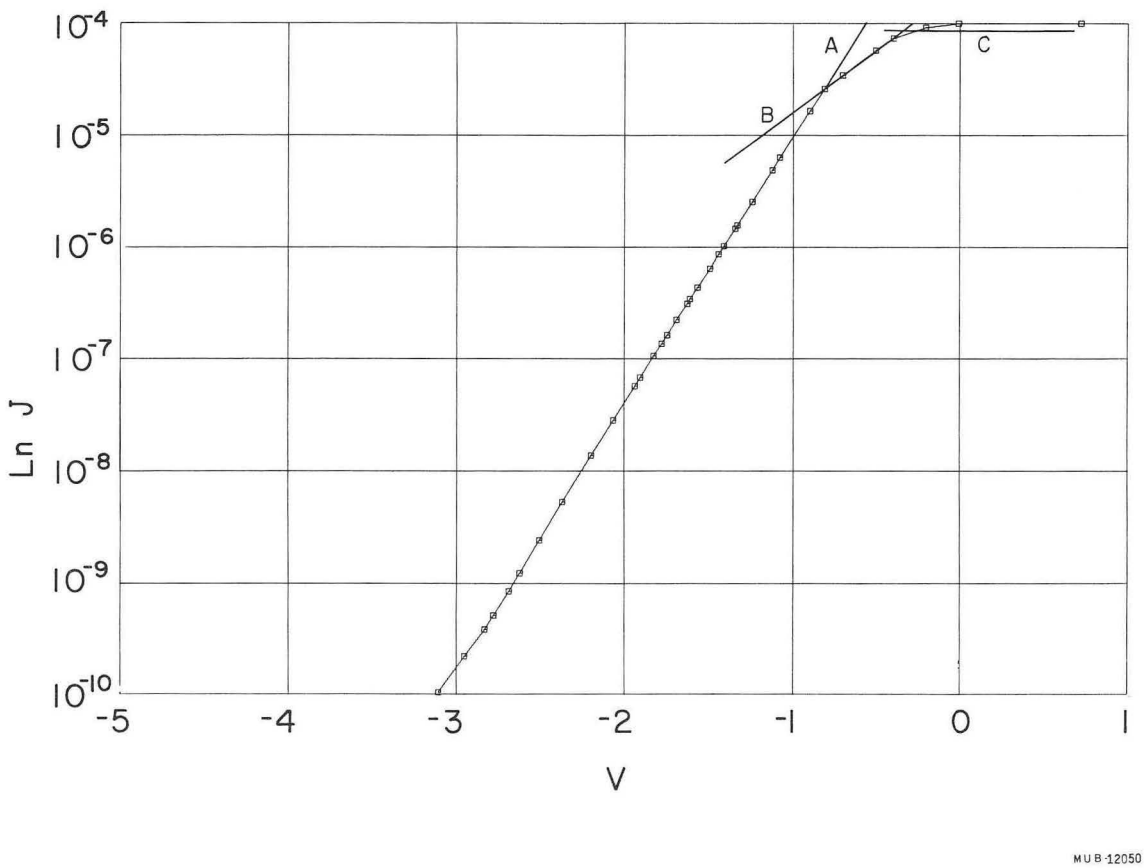

Fig. V.5

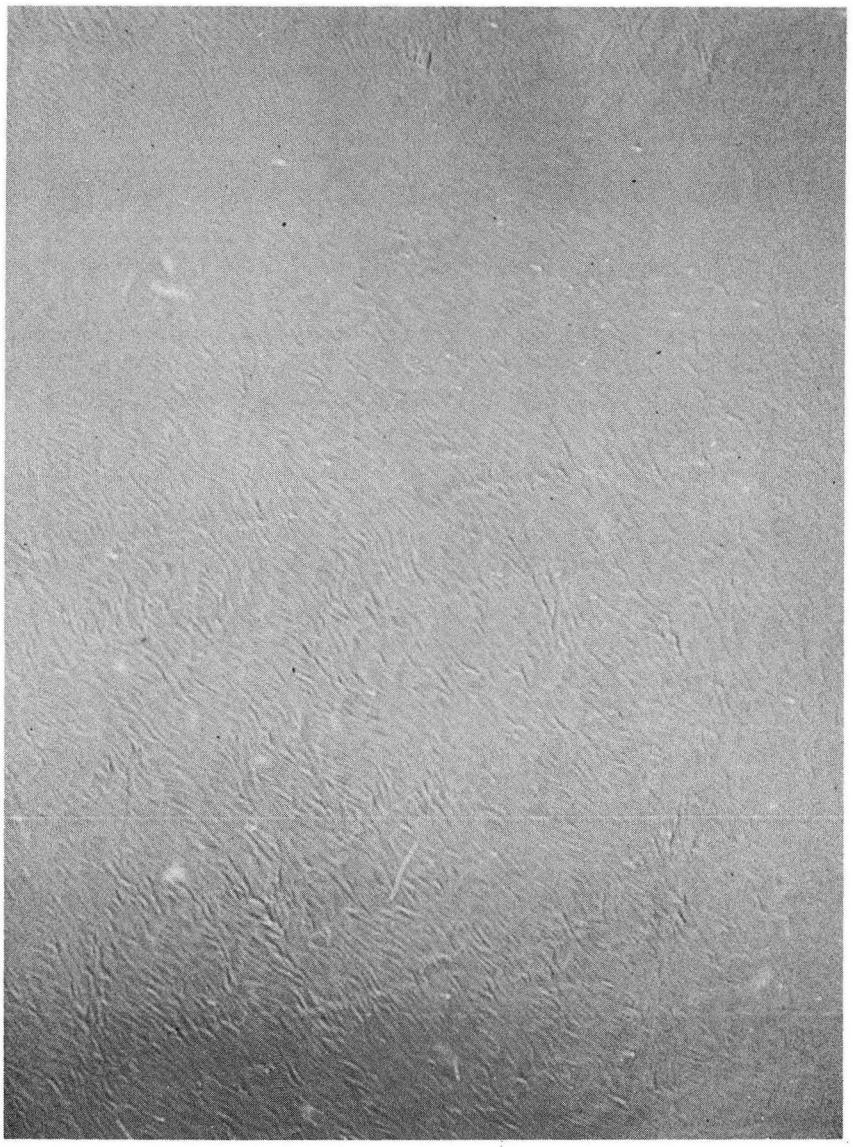

ZN-5735

Fig. V.6

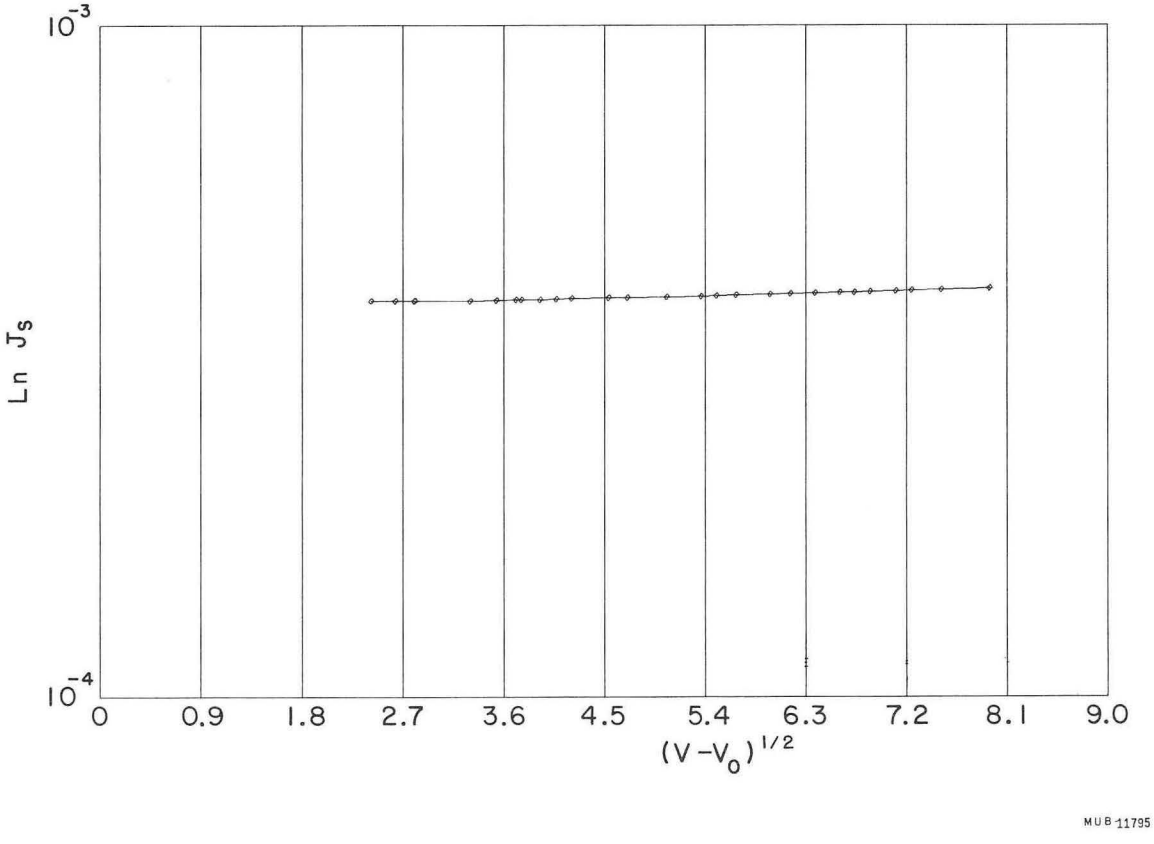

Fig. V.7

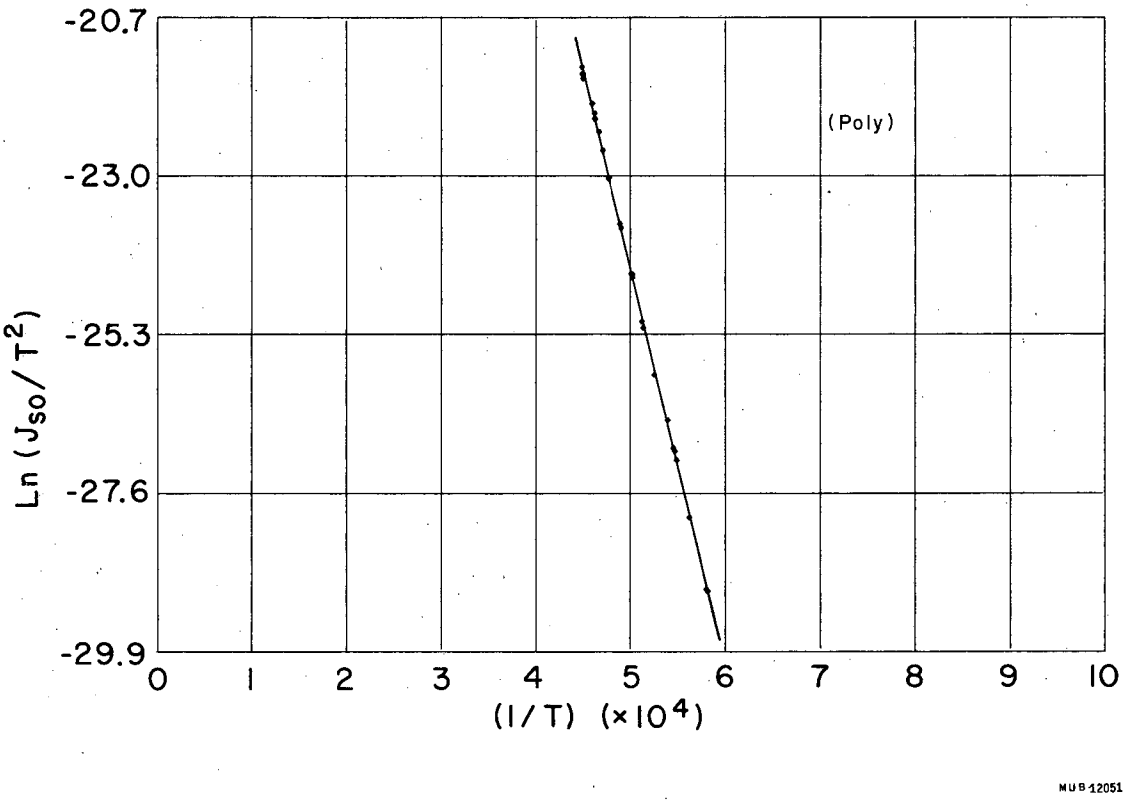
-20.7
-23.0
-25.3
-27.6
-29.9
Ln (J_{so}/T^2)
0
1
2
3
4
5
6
7
8
9
10
(1/T) (×10⁴)
(Poly)
MUB 12051

Fig. V.8

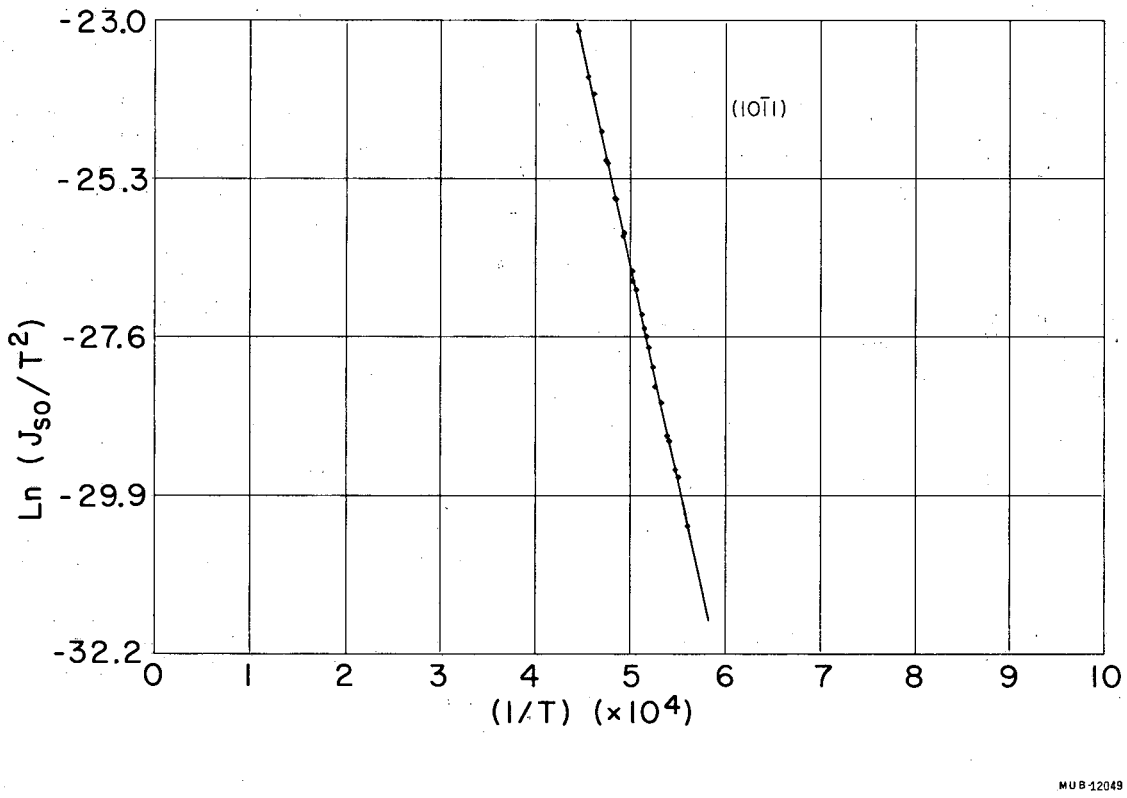
-23.0
-25.3
-27.6
-29.9
-32.2
Ln (J_{SO}/T^2)
0
1
2
3
4
5
6
7
8
9
10
(1/T) (×10⁴)
(10$\bar{1}$1)
MUB-12049

Fig. V.9

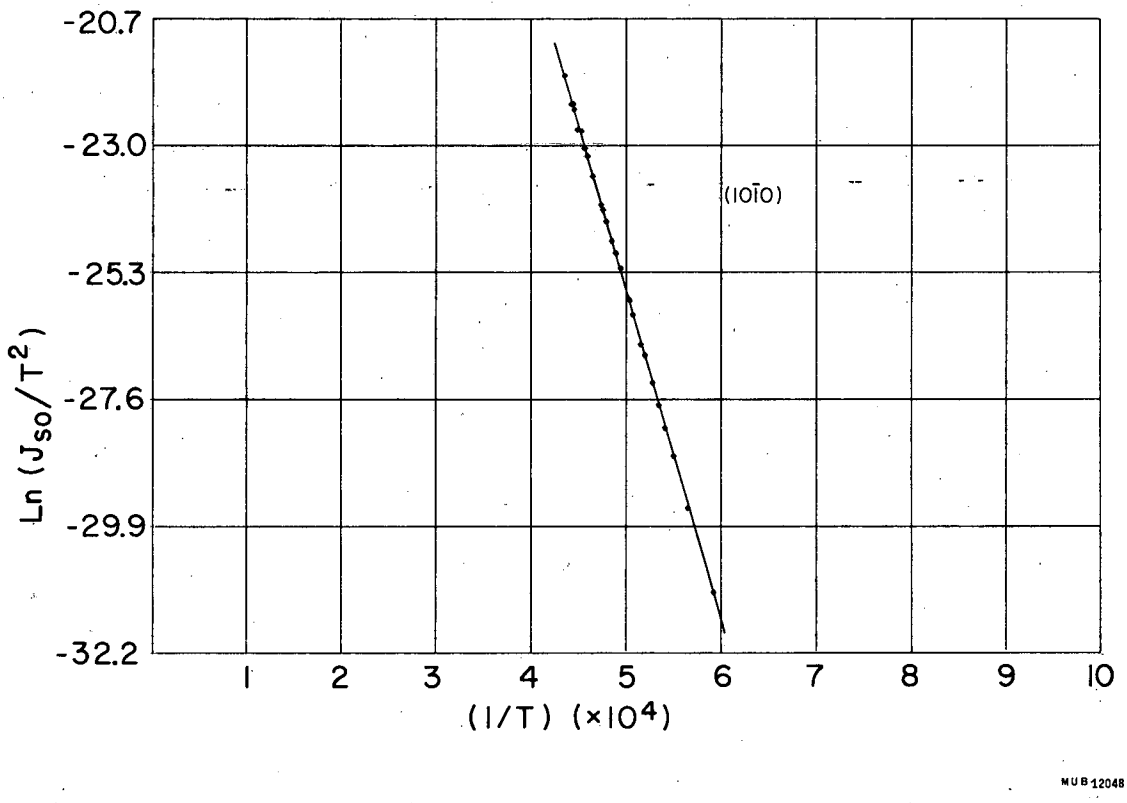
-20.7
-23.0
-25.3
-27.6
-29.9
-32.2
Ln (J_{so}/T^2)
(10$\bar{1}$0)
1
2
3
4
5
6
7
8
9
10
(1/T) (×10^4)
MUB 12048

Fig. V.10

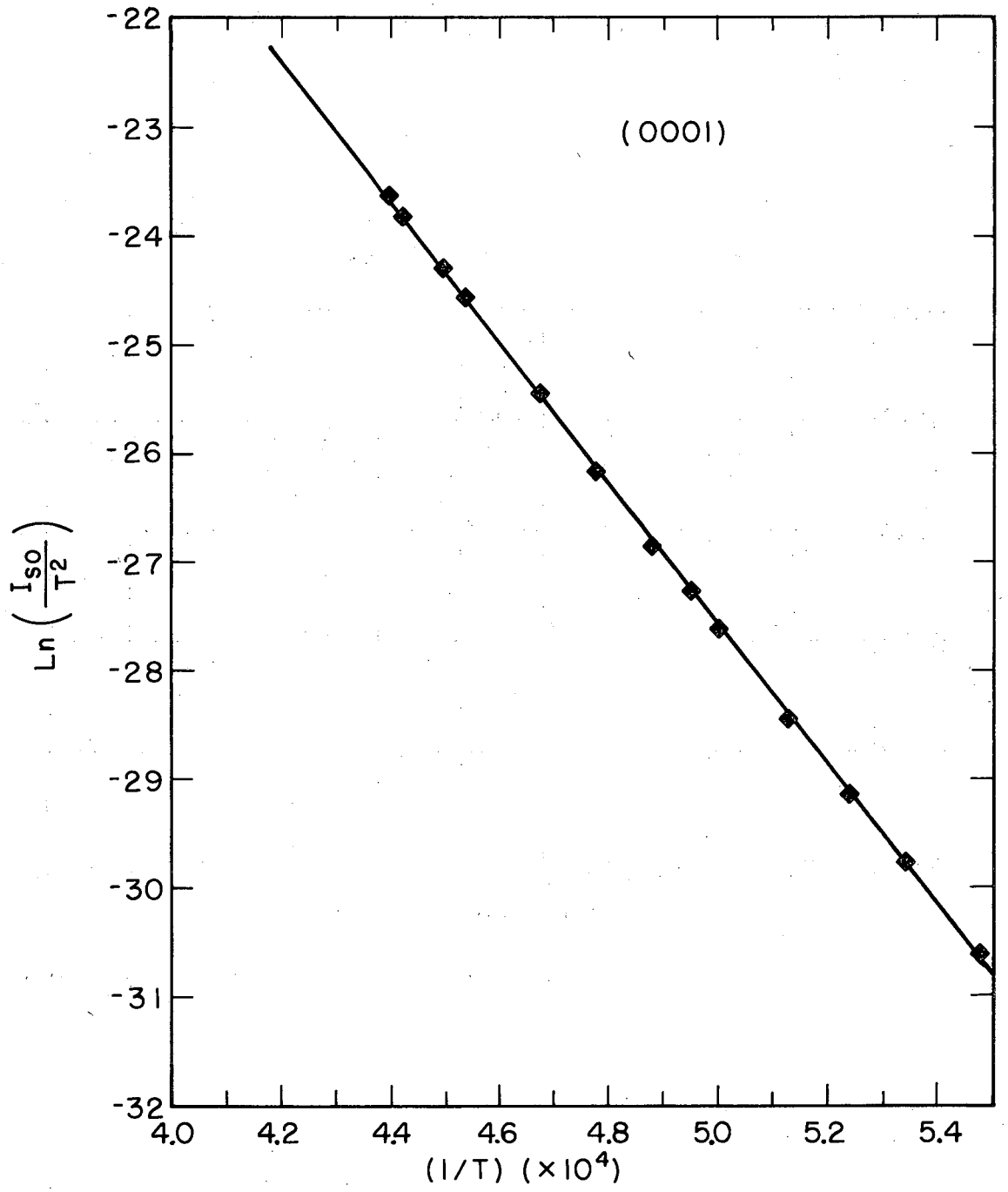

MUB 12044

Fig. V.11

B. Richardson Plots

The emission and temperature data show a linear relationship in each Richardson plot, Figs. V.8 through V.11, independent of the order in which the runs were taken. This indicates that no adsorption occurred at the emitter surface and no systematic errors developed during the runs.

The value of Φ_{poly} obtained from the Richardson plot, Fig. V.8, compares very favorably with recent literature values as shown in Table V.I. The differences in these values is probably due, in part, to the different methods of surface preparation and heat treatment used by the various authors. These different methods could result in a different distribution of work function patches, hence a different average work function. In addition, whereas the determination of the work function by thermionic means weights the areas with low work functions more heavily, the determination of Φ by thermal ionization weights the high work function more heavily. Thus, the value of Φ_{poly} obtained by Weierhausen[31] is somewhat higher than the other values in Table V.I.

Direct comparison of $\Phi_{(10\bar{1}0)}$, $\Phi_{(10\bar{1}1)}$, and $\Phi_{(0001)}$ with other values in the literature could not be done as it appears that there are no prior measurements of the bare work function for any monocrystalline rhenium surface. Table V.II summarizes the results obtained in these experiments.

The work function, $\Phi_{(0001)}$, was found to be the highest of the three determined, as was expected from the theoretical considerations discussed in Sec. II.B. This emitter actually consisted of several patches. After the emitter was brazed to the tantalum support cup, it was noted that around the edge of the emitter several new grains had formed. However, by proper centering, that portion of the emitter opposite the

Table V.I

Recent Literature Values of Φ_{poly}

Φ, ev	A, amps/($cm^2 {}^\circ K^2$)	Temperature, °K	Date	Reference
4.95	120	-	1961	26
5.07	95	2140-2544	1962	6
4.85±.05	66±20	~1470-2130	1963	27
4.65	-	1733-1903	1963	28
4.86±.04	120	1855-2144	1964	29
5.05	120	1873	1964	30
5.2	-	2000-2400	1965	31
4.96±.05	120	1325-2250	1965	32
4.93±.02	74±21	1720-2231	1966	*

* This work.

Table V.II
SUMMARY OF EXPERIMENTAL RESULTS

Surface	Poly	$(10\bar{1}0)$	$(10\bar{1}1)$	(0001)
Number of temperatures	25	26	25	13
Total number of measurements	30	26	26	17
Temperature range °K	1720-2231	1688-2291	1784-2248	1826-2277
Richardson work function and A_r value	$\Phi = 4.93\pm.02$ $A_R = 74\pm21$	$\Phi = 5.15\pm.02$ $A_R = 76\pm21$	$\Phi = 5.37\pm.03$ $A_R = 119\pm40$	$\Phi = 5.59\pm.05$ $A_R = 199\pm49$
α, temperature dependence of Φ-				
From shift in V_o	$0\pm0.7\times10^{-4}$ ev/°K	$-(1.4\pm1)\times10^{-4}$ ev/°K	$-(1.1\pm.4)\times10^{-4}$ ev/°K	$-(0.35\pm.2)\times10^{-4}$ ev/°K
Calculated from A_R	$.5\pm.3\times10^{-4}$ ev/°K	$(.4\pm.3)\times10^{-4}$ ev/°K	$(0\pm.35)\times10^{-4}$ ev/°K	$-(.4\pm.2)\times10^{-4}$ ev/°K
Φ_C	$4.30\pm.04$	$4.73\pm.10$	$4.21\pm.15$	$4.77\pm.07$
V_o	$-.63\pm.03$	$-.54\pm.04$	$-.93\pm.05$	$-0.80\pm.01$
$\Phi_C - V_o = \Phi'$	$.5\pm.3\times10^{-4}$ ev/°K	$(.4\pm.3)\times10^{-4}$ ev/°K	$(0\pm.35)\times10^{-4}$ ev/°K	$-(.4\pm.2)\times10^{-4}$ ev/°K
$(T_{calc}-T_{obs})$°K retarded region	63 ± 40	81 ± 20	46 ± 25	34 ± 22

collector consisted mostly of the undeformed (0001) orientation. By assuming a two-patch distribution at the surface, as described analytically in Appendix C, the contribution of the (0001) orientation to the total current was determined and $\Phi_{(0001)}$ obtained. The work function of the other patch(es) seen by the collector was determined to be 5.08 ± .03 ev. The orientations associated with this value were not determined. The area associated with the (0001) orientation is estimated to be more than 90% of the total area seen by the collector. The value of the work function of the (0001) orientation, obtained from the Richardson plot, agrees very well with that obtained from V_o and Φ_c as described below.

The work function of the $(10\bar{1}1)$ orientation is somewhat lower than $\Phi_{(0001)}$, as was expected. This value agrees, within experimental error, with the work function calculated from V_o, described below.

On the basis of the criteria of number of nearest neighbors of a given atom on the surface, as discussed in Section II.B, the $(10\bar{1}0)$ work function should be about the same as that of the $(10\bar{1}1)$ orientation. On the basis of packing density at the surface the $(10\bar{1}0)$ value should be higher than that of the $(10\bar{1}1)$ orientation. However, our experimental value for $(10\bar{1}0)$ rhenium lies slightly below that of $(10\bar{1}1)$ rhenium. Whether surface "smoothing" could account for this reordering, as Smoluchowski found for (112) tungsten, has not been determined.

Some further question as to the accuracy of the value for the $(10\bar{1}0)$ work function arises from consideration of Webster's[33] experiments on $(10\bar{1}0)$ rhenium immersed in cesium, where the effective work function was measured in the region of considerable depression in the surface work function due to cesium adsorption. By means of a theory

proposed by Rasor and Warner,[34] the Webster measurement extrapolates to an estimated value of about 5.7 ev for bare $(10\bar{1}0)$ rhenium, as compared to the value of 5.15 ev measured in the present experiments. The validity of the Rasor-Warner theory for such extrapolation is, however, quite questionable.

Comparison of Webster's[35] measurements on $(10\bar{1}0)$ and $(10\bar{1}1)$ rhenium in cesium may raise some further question as to the relative values of the $(10\bar{1}0)$ and $(10\bar{1}1)$ work functions for bare rhenium obtained in the present experiments. Webster found that the maximum electron emission current, obtained by varying emitter temperature at a given cesium pressure is greater for the $(10\bar{1}1)$ orientation. The Rasor-Warner theory predicts that, for surfaces with bare work functions above about 5 ev, the surface with the greater peak electron emission, at a given cesium pressure, should have the greater value for its bare work function. The validity of the Rasor-Warner theory for such extrapolation is, however, highly doubtful. Webster's experiments unfortunately did not extend far enough into the range of increasing ratio of emitter temperature to cesium temperature to provide a meaningful comparison to the present experiments.

Further question arises from a microphotograph of the $(10\bar{1}0)$ surface obtained upon completion of the emission experiments. As shown in Fig. V.6 the surface appears somewhat textured, as contrasted to the visually smooth surface prior to the experiment. Such texturing was not observed on the other monocrystalline surfaces used in these experiments. If this apparent deformation was accompanied by any significant crystallographic reorientation, ut must have occurred when the emitter was first heated, and prior to the emission measurements. Otherwise, a break or curvature in the Richardson line for this emitter would have been observed.

In summary, the measurements for $(10\bar{1}0)$ rhenium appear to have essentially the same precision as those for the other orientations. Until further experiments are carried out with bare $(10\bar{1}0)$ rhenium, there are no means at present of determining the significance of the possible doubts as to the accuracy of this measurement.

The values of A_r obtained from the Richardson plots vary from 74±21 to 199±49, as seen in Table V.II, and the dependence of the work function on temperature, α, calculated from A_r, using Eq. (II.3), is in the range of 10^{-4} ev/°K, a typical value for clean metal surfaces.

C. Shelton Plots

As discussed in Section IV.B, the temperature of the collector was maintained at 150°C ±25°C throughout each of the experiments. From the Shelton plots, no systematic variation in Φ_c could be observed within the small variation of collector temperature in these experiments. However, Φ_c calculated from the first (poly) set of runs and the third $(10\bar{1}1)$ set of runs is 4.25 ev, as compared with 4.75 ev from the second $(10\bar{1}0)$ and fourth (0001) set.

These values differ from the value of 5.61 ev[36] for the bare work function of (100) copper because, after the first set of runs, the collector surface was observed to be covered with a bluish deposit, which was not subsequently removed. The variation in Φ_c calculated from the Shelton plot is ascribed to the fact that for the 2nd and 4th set of runs, the emitter was baked out above 2000°C, whereas for the 1st and 3rd sets of runs the maximum emitter temperatures were less than 2000°C. It is probable that material evaporated from the hotter parts of the diode was responsible for the bluish deposit and the change in work function.

As discussed in Section II , the values of A obtained from the Shelton plot should be the theoretical value of 120 amps/cm^2°K^2, if Φ_c was held constant, and if the calculated temperatures for the retarded regions were equal to the observed temperatures. Although Φ_c was held constant, the calculated temperatures differed from the observed temperatures as indicated in Table V.II.

An obvious reason for this difference is that the temperature measured was lower than the true temperature, as a result of increased absorption in the viewing port because of an evaporated film onto the glass. The measured temperature could also have been lower than true temperature if the hohlraum in the emitter did not represent black-body conditions.

The difference between calculated and observed temperatures showed no noticeable increase as the experiments continued. In addition, the power input necessary for each emitter temperature was monitored, and no increase in power was needed to bring the emitter to the same temperature at the end as at the beginning of the runs. This indicates that absorption in the window did not increase over the amount compensated for by calibration.

The geometry of the hohlraum was such that the length to width ratio was in excess of 6:1. This ensured that the temperature read at the hohlraum was the black-body temperature.[37] However, if the knee of the ln J-V curve was rounded or shifted in the positive (voltage) direction, this would have the effect of decreasing the slope of the retarded region, hence increasing the calculated temperature. This rounding in the knee can come about as the result of a non-uniform work function of the emitter or collector surface, as a result of space charge, geometry effects, or reflection at either of the electrode surfaces.

Another possible reason for the temperature differences is the reflection of low energy electrons from the emitter and collection surfaces. This phenomena would result in an increase in the temperature calculated from the slope of the retarded region.[15]

The Shelton plots resulted in A values of 94±36, 48±42, 217±186, and 143±93 amps/cm^{2}°K^{2} for the (poly), $(10\bar{1}1)$, $(10\bar{1}0)$, and (0001) emitters, respectively.

As shown by Eq. (II.7), the work function of the emitter can be obtained from the knee of the I-V curve and from Φ_c. As shown in Talbe V.II, the values of Φ obtained from Φ_c and V_o for each of the emitters agree, within experimental error, with the values of Φ obtained from the Richardson plot. However, because of the lack of precision of the values of Φ_c and V_o obtained from the Shelton plot, the work functions obtained from the Richardson plots are preferred.

VI. CONCLUSIONS

These experiments were designed to determine the work function of polycrystalline and monocrystalline rhenium. A planar geometry, guarded-collector vacuum thermionic diode was built, and data obtained for the polycrystalline and $(10\bar{1}0)$, $(10\bar{1}1)$ and (0001) surfaces of rhenium in the temperature range, 1400-2000°C. The work functions were obtained from a Richardson plot. In addition, the work function of the monocrystalline copper collector was determined by means of a Shelton plot and from this value and the value of the knee of the ln J-V curves, work functions of the emitters were obtained which compared favorably with the Richardson work functions.

Table V.II summarizes the results and precision of measurements obtained in these experiments.

Some doubt as to the accuracy of the work function of the $(10\bar{1}0)$ orientation exists, because of inferrences from the value of the cesiated work function obtained elsewhere for this orientation.

ACKNOWLEDGMENTS

I wish to express my thanks and deep gratitude to:

Professor T. H. Pigford, for introducing me to the field of thermionics, for his continuous support and for his critical review of this work;

Professors H. P. Smith, Jr. and E. R. Parker, for their time and effort spent in reviewing this work;

Dr. D. R. Koenig, for, among numerous other things, the basic design of the diode, for his many thought-provoking questions and fruitful discussions with me;

Mr. S. S. Schreiner, for his more than considerable help in building the vacuum system and thermionic diode;

Messrs D. J. Sikkema and A. Arthur, for their invaluable assistance with the electronics;

Misses E. Williams and E. Coleman, for their help in devising the Therm II and Resist computer programs;

and Dr. L. D. Posey, who, by his encouragement and example, inspired me.

More than thanks and gratitude, I owe to my wife, Perla. Without her patience, encouragement, assistance and love, this work would have been longer yet in coming.

I would also like to express my appreciation to the Oak Ridge Institute of Nuclear Studies for fellowships received during the early part of this work.

This research was performed under the auspices of the Atomic Energy Commission.

NOMENCLATURE

A	theoretical constant in Richardson Equation = 120.4 amps/cm^2-°K
A_r	Richardson "A" value obtained from intercept of Richardson plot
e	electron charge
F	field between emitter and collector, volts/cm
I	current, amps
J	current density, amps/cm^2
k	Boltzmann constant
r	radius of shell about a given atom
R	resistance, ohms
T	temperature, °K
T_o	minus 273 °K
V	voltage of emitter relative to collector, volts
V_d	decelerating voltage (for electrons) between emitter and collector, volts
α	temperature dependence of the work function, ev/°K
ϵ_o	permittivity of free space
Φ	emitter work function
Φ'	temperature and field dependent emitter work function, ev
Φ''	field-dependent emitter work function, ev
Φ_c	collector work function, ev
ρ	density - grams/cm^3

Subscripts

s	value in the saturated region
so	field-free saturated value

APPENDIX A.

Electropolishing Solutions

The following electropolishing recipes for rhenium, obtained from the various sources mentioned, are listed in order of their effectiveness (as determined by the author) in producing pit-free surfaces.

1. Solution: 350 ml absolute ethanol
   175 ml perchloric acid (ρ = 1.54)
   50 ml butoxy ethanol (Butyl Cellosolve)

   Cathode: Pt wire

   Voltage: 50 volts

   Current Density: 6 amps/cm^2

   Source: G. A. Geach, et al., "Rhenium" ed. B. W. Gonser, Elsevier Publishing Co., New York, 1962, p.85.

   Remarks: This solution appears to be the most universally used, with different voltages and current densities used for different orientations. Unfortunately, so far as we have been able to determine, consistent results are difficult to obtain. In our experiments, reasonably pit- and etch-free surfaces have been obtained at ~13 volts for polycrystalline rhenium and the $(10\bar{1}0)$ orientation and at 22 volts for the $(10\bar{1}1)$ orientation, at current densities near 5 amps/cm^2.

2. Solution: 75 volume percent absolute ethanol
   25 volume percent 36N sulfuric acid

   Cathode: Stainless Steel

Voltage: 20 to 30 volts

Current Density: 1 to 2 amps/in^2

Temperature: About 70°F

Source : J. Bergin, J. G. Beach, Battelle Memorial Institute, Columbus, Ohio, private communication.

3. Solution: 5 volume percent Sulfuric Acid

1-1/4 volume percent Hydrofluoric Acid

Remainder: Methyl Alcohol

Voltage: 50 volts

Source: F. W. Reynolds, Lawrence Radiation Laboratory, Berkeley, California, private communication

4. Solution: 6 ml Perchloric Acid (62%)

600 ml Methanol

360 ml Butyl Cellosolve

trace wetting agent

Voltage: 50 to 60 volts

Current Density: 2 amps/cm^2

Needs Stirring

Source: F. W. Reynolds, ibid.

APPENDIX B.

CHEMICAL ANALYSIS AND LAUÉ X-RAY PICTURES OF RHENIUM

The polycrystalline rhenium was obtained from the Rembar Sales Corporation. It was formed into a rod 5/8" in diameter from 99.99% pure powder. Table B.1 presents a chemical analysis for this material.

The monocrystalline rhenium was purchased from Union Carbide, Linde Division. One piece, 5/8" in diameter and 2" long was grown and zone-refined from 99.99% pure rhenium. No analysis is available for the monocrystalline material.

Figures B.1, B.2 and B.3 show the back-reflection Laué x-ray pictures obtained from each of the orientations selected for use in the thermionic diode.

TABLE B.1

CHEMICAL ANALYSIS OF POLYCRYSTALLINE RHENIUM

Impurity	
Al	< .0005%
B	.0001
Ca	.0001
Co	.0003
Cr	.0003
Cu	.0002
Fe	.0050
Mg	.0001
Mn	.0002
Mo	.0025
Ni	.0001
Sn	.0002
Ti	.0002
Zr	.0002
Na	.0001
K	.0001
Non Metallic	
C	.0020%
Si	.0003
H	.0005
N	.0010
O	.0040

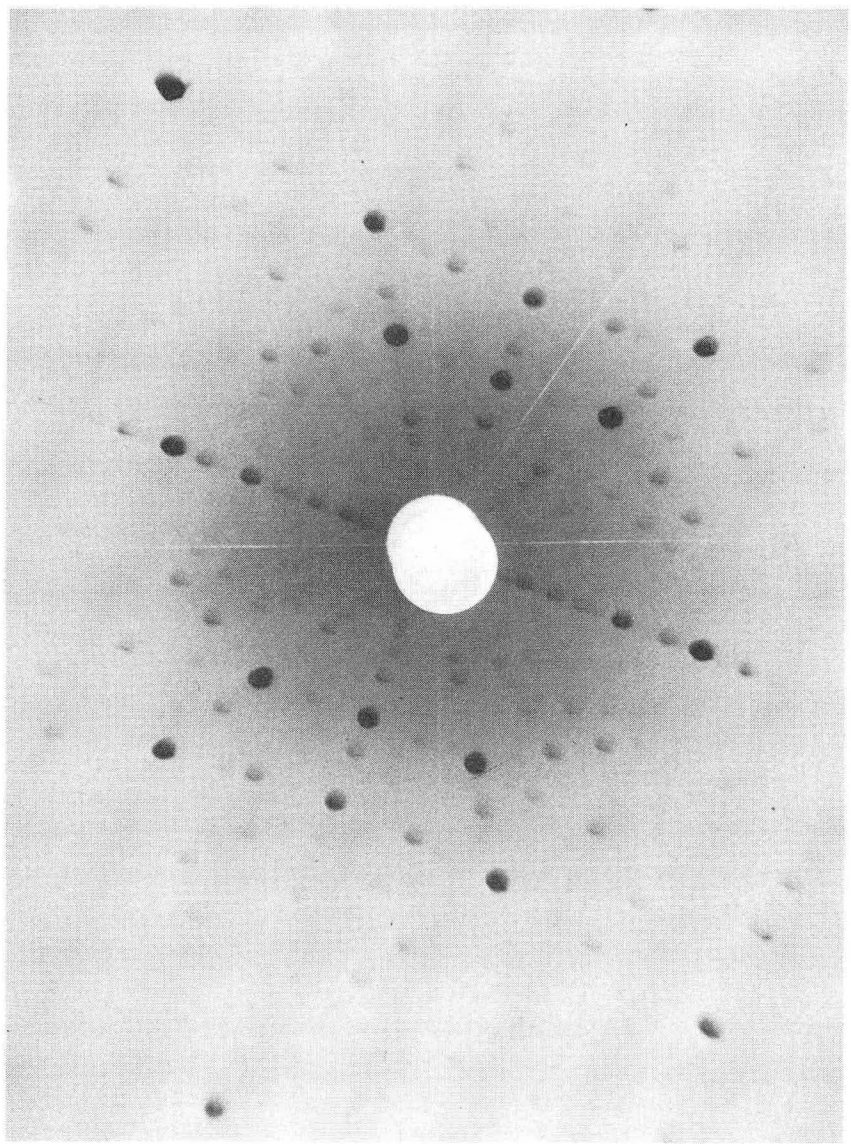

ZN-5733

Fig. B.1

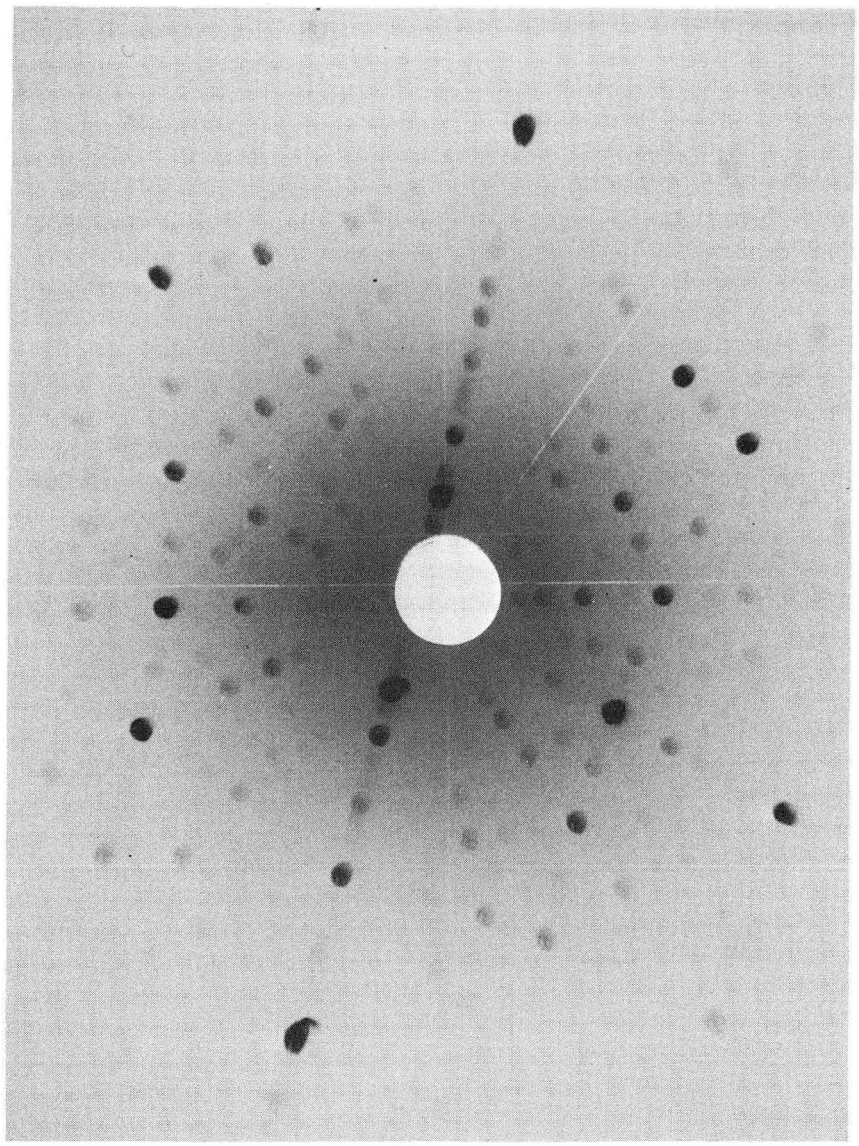

ZN-5737

Fig. B.2

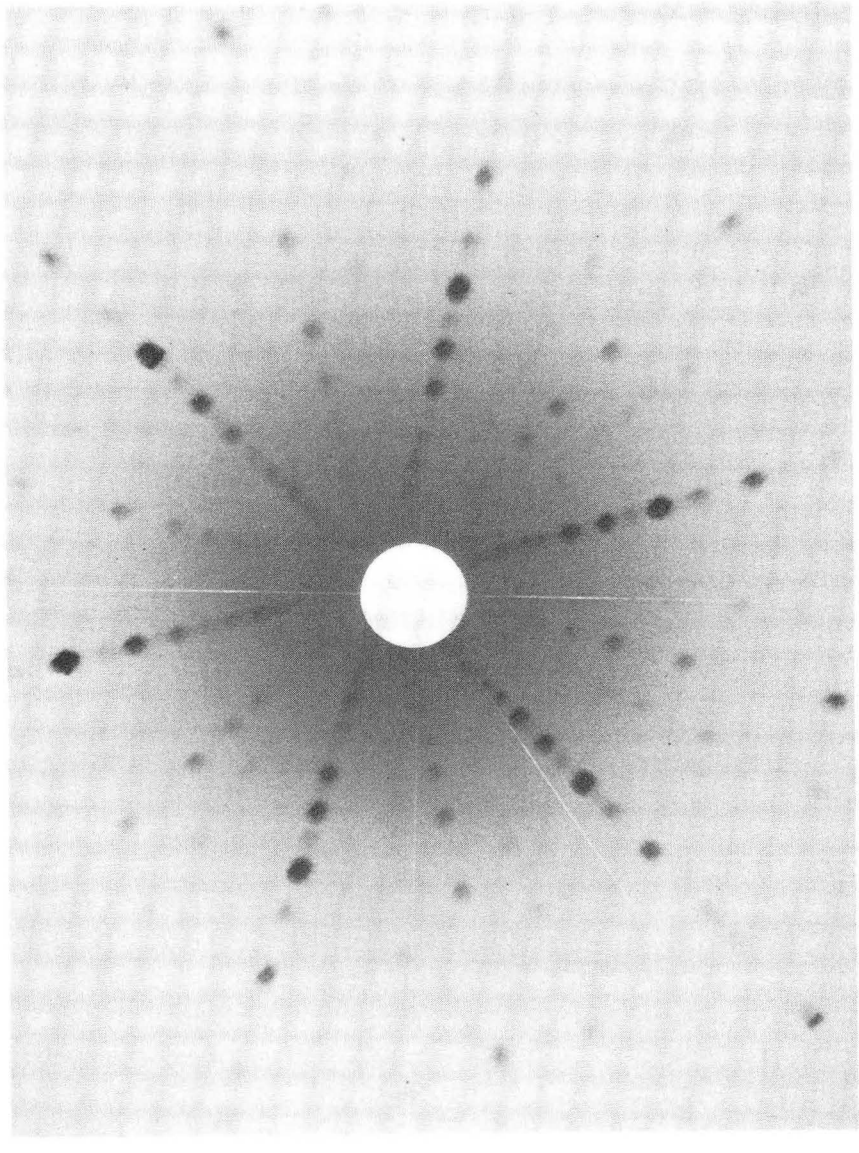

ZN-5734

Fig. B.3

APPENDIX C.

THE TWO-PATCH CURRENT-VOLTAGE CHARACTERISTIC

The two-patch I-V curve can be characterized by three regions; a retarded and a saturated region, and a region whose slope has a value between the retarded and saturated regions, as in Fig. C.1. Curves 1 and 2 represent the current-voltage characteristic of each of the two regions, with $\Phi_2 > \Phi_1$. Hence the two-patch current is simply the sum of each of the currents I_1 and I_2 at each voltage i.e.,

$$I_1(V) + I_2(V) = I(V). \tag{C.1}$$

Thus we have

$$I_{so} = I_{so1} + I_{so2}. \tag{C.2}$$

By assuming that V_{o_1} is not much smaller than V_{o_2}, we can say that

$$I_1(V') = I_{so_1} \quad (V_{o_1} \leq V' \leq V_{o_2}) \tag{C.3}$$

(This assumption is valid for the analysis of the (0001) data, since $(V_{o_1} - V_{o_2})$ was approximately one-half volt. This resulted in a low enough electric field that the Schottky correction to I_1 from V_{o_2} to V_{o_1} can be neglected.)

In the retarded region of curve 2, we have

$$I_2(V') = I_{so_2} \exp \left\{\frac{e}{kT}(V' - V_{o_2})\right\} \tag{C.4}$$

or from Eqs. C.1, C.3 and C.4,

$$I(V') = I_1(V') + I_{so_1} + I_{so_2} \exp \left\{\frac{e}{kT}(V' - V_{o_2})\right\} \tag{C.5}$$

Combining Eqs. (C.2) and (C.5) we get

$$I(V') = I_{sol} + (I_{so} - I_{sol}) \exp\left\{\frac{e}{kT}(V' - V_{o_2})\right\} \qquad (C.6)$$

or

$$I_{sol} = \frac{I(V') - I_{so} \exp\left\{\frac{e}{kT}(V' - V_{o_2})\right\}}{1 - \exp\left\{\frac{e}{kT}(V' - V_{o_2})\right\}} \qquad (C.7)$$

Therefore we can obtain Iso_1 if we know V_{o_2}, I_{so}, and the current at a given voltage, V' between V_{o_1} and V_{o_2}. Knowing Iso, we can find Φ , and in principle, if we can obtain the area of patch 1 then we can obtain a value for the current density, and from that the Richardson "A" value, A_r.

Table C.I and Fig.V.2 present the results of Eq.(C.7) applied to the (0001) data.

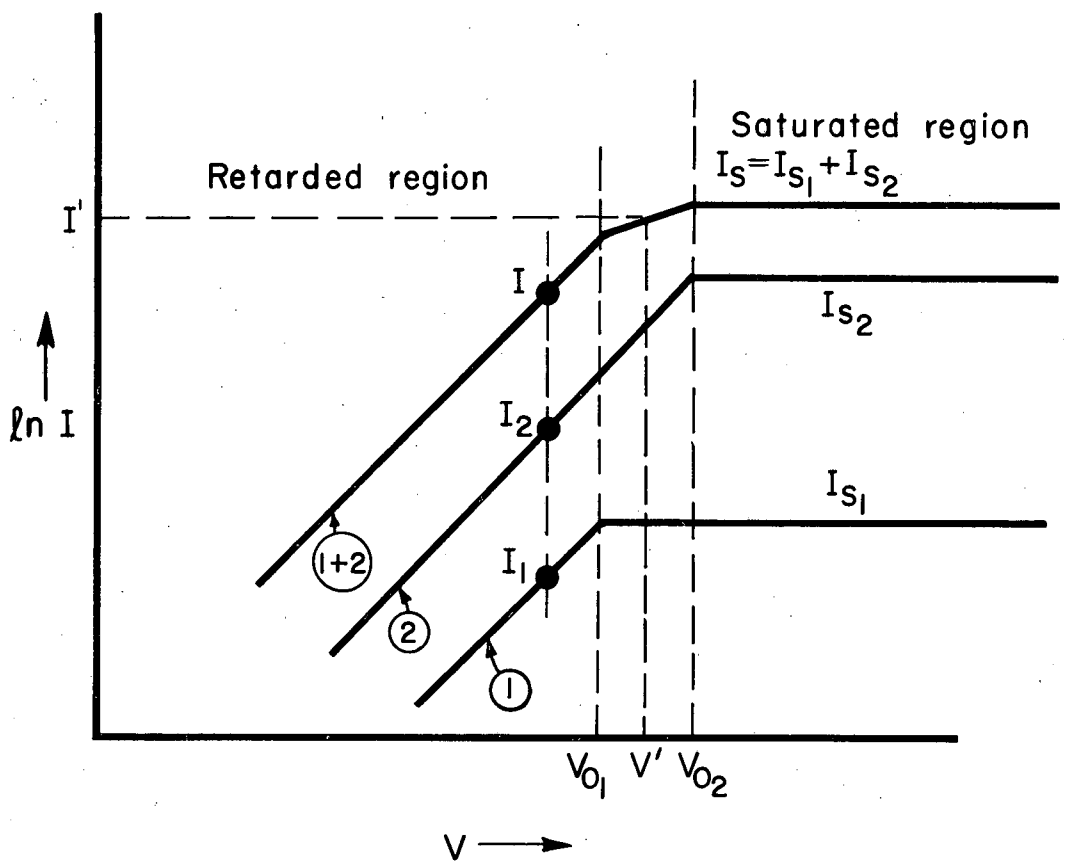

MUB 12043

Fig. C.1

Table C.I

Analysis of (0001) Data, Assuming a Two-Patch Emitter Surface

Run No.	Temp. °C	Iso, amps	V_{o_1}, volts	V_{o_2}, volts	Iso_1, amps
102	2004	7.259×10^{-4}	-.80	0	2.88×10^{-4}
104	1988	5.978×10^{-4}	-.79	-.12	2.32×10^{-4}
119	1964	4.109×10^{-4}	-.80	-.17	1.716×10^{-4}
106	1932	2.968×10^{-4}	-.80	-.24	1.032×10^{-4}
121	1871	1.348×10^{-4}	-.81	-.29	6.16×10^{-5}
107	1868	1.302×10^{-4}	-.81	-.29	4.14×10^{-5}
108	1820	6.496×10^{-5}	-.80	-.33	1.882×10^{-5}
110	1776	3.404×10^{-5}	-.81	-.35	9.05×10^{-6}
126	1738	2.142×10^{-5}	-.82	-.33	6.66×10^{-6}
125	1738	2.135×10^{-5}	-.83	-.35	5.85×10^{-6}
123	1738	2.134×10^{-5}	-.83	-.35	5.75×10^{-6}
111	1725	1.595×10^{-5}	-.80	-.33	3.96×10^{-6}
113	1678	7.189×10^{-6}	-.81	-.34	1.666×10^{-6}
112	1677	7.199×10^{-6}	-.81	-.34	1.665×10^{-6}
115	1636	3.582×10^{-6}	-.81	-.34	8.02×10^{-7}
116	1599	1.883×10^{-6}	-.81	-.31	4.22×10^{-7}
117	1553	7.937×10^{-7}	-.81	-.33	1.691×10^{-7}

APPENDIX D

Data Reduction Programs and Error Analysis

1. Two computer programs were developed for use in analyzing the data with the aid of the CDC 6600 computer at the Computer Center at LRL-Berkeley. Both programs are in Fortran IV.

The first of the two, "Resist", was developed for a two-fold purpose. It first takes the raw input data which contains the current and voltage information in the form of 16 digits (0-9) and converts it to the proper form (punched IBM cards) for use with Therm II, the program which computes the work function, etc; as described below.

Second, as part of the input raw data, a set of current and voltages corresponding to leakage currents is fed into it and this program subtracts the proper leakage current from each of the measured currents obtained during a run. If the measured current is obtained at a voltage different from a voltage in the leakage data, then the program interpolates between the leakage current-voltage points that it has, and subtracts the linearly interpolated current from the raw input current.

Program Set-up:

Card 1: Format (8A10)

Values of collector resistors 1 through 8.

Card 2: Format (22X, F7.2)

Temperature card corresponding to leakage data, T = 9999.

Card 3 + (N'-1) (N' = number of leakage data cards)

Format (2(2I1, I2, I6, I3, I1, I8, 7X), 2I1, I2, I6, I3, I1, I8)

Leakage data

Card N' + 3: Blank

This is a control card which indicates the last data card has been read for a given set.

Card N' + 4:

Format (22X, F7.2)

Temperature card, identifying a given run

Card N' + 4 + (M' - 1):

Format (2(2I1, I2, I6, I3, I1, I8, 7X), 2I1, I2, I6, I3, I1, I8)

Input data cards (M' = number of data cards)

Card N' + 4 + M: Blank

(Same function as card N' + 3)

As many sets of data as desired may be processed by repeating cards (N' + 4) to (N' + 4 + M').

Note: An additional blank card must follow the last data set. This card signifies that control is to be returned to the main program for processing other steps.

Output: Punched Cards

Format: (6E12.5)

Current-voltage values, corrected for leakage currents. (Voltage drop across collector resistor, applied voltage, collector resistor.)

A card list for "Resist" follows:

```
      PROGRAM RESIST( INPUT,OUTPUT,TAPE2=INPUT,TAPE3=OUTPUT,TAPE14)
      DIMENSION ID(8), IC(3), JC(3), KR(3), LC(3), IV(3), JV(3), LV(3)
      DIMENSION VOLT(200,2), CURR(200,2), IRES(200,2), SUB(200)
      READ(2,1) (ID(I), I=1,8)
 1    FORMAT(8A10)
      II = 1
 7    READ(2,3) TEMP
 3    FORMAT(22X, F7.2)
      IF( ENDFILE 2) 39, 41
 41   IF( TEMP .NE. 9999. ) II = 2
      J = 1
 5    READ(2,4) (IC(I), JC(I), KR(I), LC(I), IV(I), JV(I), LV(I), I=1,3)
 4    FORMAT( 2( 2I1, I2, I6, I3, I1, I8, 7X), 2I1, I2, I6, I3, I1, I8)
      IF( IC(1) .EQ. 0) GO TO 18
      JEND = J+2
      IF( IC(3) .EQ. 0) JEND = J+1
      IF( IC(2) .EQ. 0) JEND = J
      DO6 K =J,JEND
      KJ1 = K-J+1
      ICK = IC(KJ1)
      GO TO (8, 9, 10, 11, 11), ICK
 8    WRITE(3,12)
 12   FORMAT(//, 10X, 48H AN ERROR OCCURRED IN READING THE DATA, WHEN K
     1=,I5)
      GO TO 40
 9    CURR(K,II) = FLOAT( LC(KJ1) ) / 100.
      GO TO 13
 10   CURR(K,II) = FLOAT( LC(KJ1) ) / 1000.
      GO TO 13
 11   CURR(K,II) = FLOAT( LC(KJ1) ) / 10000.
 13   CONTINUE
      IRES(K,II) = KR(KJ1)
      IVK = IV(KJ1)
      GO TO(8, 14, 15, 16, 16), IVK
 14   VOLT(K,II) = FLOAT( LV(KJ1) ) / 100.
      GO TO 17
 15   VOLT(K,II) = FLOAT( LV(KJ1) ) / 1000.
      GO TO 17
 16   VOLT(K,II) = FLOAT( LV(KJ1) ) / 10000.
 17   CONTINUE
      IF( JC(KJ1) .EQ. 1) CURR(K,II) = -CURR(K,II)
      IF( JV(KJ1).EQ. 1) VOLT(K,II) = -VOLT(K,II)
 6    CONTINUE
      J = JEND+1
      GO TO 5
 18   CONTINUE
C
C        N          NUMBER OF DATA POINTS READ IN FOR ZERO T.
C        M          NUMBER OF DATA POINTS READ IN FOR NONZERO T.
C
      IF( II .EQ. 1) N = J-1
      IF( II .EQ. 2) M = J-1
      IF( II .EQ. 2) GO TO 26
      WRITE(3,19)
 19   FORMAT(1H1, 20X, 39H INPUT DATA FOR T=0 IS AS FOLLOWS - /)
      IEND = N
```

```
27    DO20 K=1,8
      WRITE(3,21) K, ID(K)
21    FORMAT(/15X, 17H FOR RESISTOR NO., I2, 4H OR , A10, /10X, 8H CURRE
     1NT, 12X, 8H VOLTAGE/)
      DO22 I=1,IEND
      IF( IRES(I,II) .NE. K) GO TO 22
      WRITE(3,23) CURR(I,II), VOLT(I,II)
23    FORMAT( 5X, 2E20.4)
22    CONTINUE
20    CONTINUE
      IF( II .EQ. 1) GO TO 7
      GO TO 28
26    WRITE(3,25) TEMP
25    FORMAT(1H1, 10X, 19H INPUT DATA FOR T =, F8.2, 16H IS AS FOLLOWS -
     1,/)
      IEND = M
      GO TO 27
28    CONTINUE
      DO29 I=1,M
      DO30 J=1,N
      IF( IRES(I,2) .NE. IRES(J,1) ) GO TO 30
      IF( VOLT(J,1) .EQ. VOLT(I,2) ) GO TO 32
      IF( VOLT(J,1) .GT. VOLT(I,2) ) GO TO 31
30    CONTINUE
32    CUR = CURR(J,1)
      GO TO 33
31    CUR = CURR(J-1,1) + (VOLT(I,2)-VOLT(J-1,1)) * (CURR(J,1)-CURR(J-1,
     11)) / (VOLT(J,1)-VOLT(J-1,1))
33    SUB(I) = CURR(I,2) - CUR
29    CONTINUE
      WRITE(3,34)
34    FORMAT(1H1, 10X, 41H TABLE OF VOLTAGES AND CORRECTED CURRENTS/)
      DO35 K=1,8
      WRITE(3,36) K, ID(K)
36    FORMAT(//, 15X, 17H FOR RESISTOR NO., I2, 4H OR , A10, /10X, 8H CU
     1RRENT, 12X, 18H CORRECTED CURRENT, 2X, 8H VOLTAGE/)
      DO37 I=1,M
      IF( IRES(I,2) .NE. K) GO TO 37
      WRITE(3,38) CURR(I,2), SUB(I), VOLT(I,2)
38    FORMAT( 5X, 3E20.4)
37    CONTINUE
35    CONTINUE
      DO24 I=1,M
      ISUB = IRES(I,2)
      WRITE(14,42) SUB(I), VOLT(I,2), ID(ISUB)
      WRITE( 3,42) SUB(I), VOLT(I,2), ID(ISUB)
42    FORMAT( 1X, E11.4, 1X, E11.4, 2X, A10 )
24    CONTINUE
      DO2 I=1,M
      IRES(I,2) = 0
      VOLT(I,2) = 0.0
2     CURR(I,2) = 0.0
      GO TO 7
39    CONTINUE
      ENDFILE 14
40    CONTINUE
      STOP
      END
```

THERM II

2. This program was designed to reduce the raw I-V data obtained from the experimental runs and obtain a value for the work function and A_r from a Richardson plot. It was designed for use with the CDC 6600 computer.

In order to obtain the Richardson plot of $\ln J_{so}/T^2$ vs $1/T$, Jso must be calculated. As shown in Section II.A, J_{so} is the intercept of the Schottky plot. For the Schottky plot, the field, F, between the emitter and collector must be known. This means that the internal voltage between the emitter and collector, $(V_o - V)$, must be known. Therefore, in order to obtain Φ and A_r, V_o and Jso must be determined.

Therm II is composed of 5 parts, each part consisting of a least squares fit to the data, assuming linear correlations. The data included in these 5 parts are data from the retarded region, the saturated region, the Schottky plot, the Richardson plot and the Shelton plot.

The output of the program is in two parts: print-out sheets and plotted curves, obtained with the aid of a Cal-Comp plotter.

In order to find V_o for a given temperature run, the program assumes that the retarded region ((1) in Fig. II.1) can be expressed by Eq. (II.6),

$$J = J_{so} \exp\left\{\frac{e}{kT}(V - V_o)\right\} \qquad \text{(D.1)}$$

It then calculates the best fit to selected points in this region. In addition, it finds the best straight line through selected points in the saturated region. The intersection of these two lines yields V_o, as shown in Fig. II.1 .

Having calculated V_o, the program then proceeds to calculate J_{so} by means of the Schottky plot. Selected points are fitted to the expression,

$$J_s \sim J_{so} \quad \exp \left\{ \frac{(V - V_o)^{1/2}}{T} \right\} \tag{D.2}$$

which results from Eq. (II.4) for a constant diode spacing d. This does not affect the value of the intercept, J_{so}. The temperature can be found from the slope by multiplying the latter by $\frac{e}{k} \left(\frac{1}{d}\right)^{1/2}$.

Thus with J_{so} found for each run at temperature T, a best fit to the Richardson plot can be obtained. As mentioned above, the slope and intercept of this fitted line yields Φ and A_r.

The last part of Therm II calculates the current density, J, form each of the runs, at a given voltage in the retarded region. As shown in Section II.A, a plot of $\ell n\ J/T^2$ vs $1/T$, where J is calculated at a given value of V in the retarded region, is the Shelton plot. From the slope of the best fitted line we can obtain the collector work function, Φ_c, and, as shown in Section II.A, if the collector work function was kept constant, then the work function of the emitter, Φ, may be obtained.

PROGRAM SET-UP

A. INPUT

CARD 1: FORMAT (I5)

NVCOL = no. of collector potentials used, that is, the no. of Shelton plots to be made. $0 < NVCOL \leq 10$

CARD 2: FORMAT (6E12.5)

VCOL (I), I = 1, NVCOL = collector potentials used for

CARD 3: FORMAT (6E12.5)

TEMP = temperature

IN = noise current

XMAX = maximum value of abscissa used for plotting

XMIN = minimum value of abscissa used for plotting

A = area of diode

DELX is a number such that $\left(\frac{XMAX - XMIN + .5}{DELX}\right)$

is the number of vertical grid lines on graph of current density versus voltage.

CARD 4: FORMAT (6E12.5)

VRMIN = minimum retarding region potential for plot.

VRMAX = maximum retarding region potential for plot.

VSMIN = minimum saturated region potential for plot.

VSMAX = maximum saturated region potential for plot.

VSCMIN = minimum potential for SCHOTTKY plot.

VSCMAX = maximum potential for SCHOTTKY plot.

CARD 5 - CARD 4 + (N-1): FORMAT (6E12.5): (N = no. of data points)

I' = voltage across known resistor.

V = voltage

R = resistance

CARD 4 + N: BLANK

As many data sets as desired may be processed at execution time by repeating from CARD 3.

NOTICE: An additional Blank card must follow the last set of data.

B. OUTPUT

For each data set, the following output is given:

Line 1: TEMP, IN, XMAX, XMIN, A, DELX

Line 2: - Line N + 1: I_i', V_i, R_i, i = 1, N

Line N + 2: $\log_e [(I_i') R - IN]/A$, V for all data points such that the $\log_e$ quantity > 0.

Next Line: Initial temperature in degrees Kelvin. Next output is a least squares fit of data points in the retarded region followed by the fitted temperature. Then comes the least squares fit of the data points in the saturated region and the corresponding fitted voltage, V_o. Lastly is the fitted data points for the SCHOTTKY plots and the corresponding fitted current density.

End of output for each data set.

If there are two or more sets of input data then a least squares fit is made for those data points corresponding to the Richardson plot and NVCOL least square fits for the data points corresponding to the SHELTON plot.

In addition to the above output there are three plots for each set of data and (NVCOL + 1) additional Plots.

CARD LIST FOR THERM II:

```
      PROGRAM THERMII(INPUT,OUTPUT,TAPE2=INPUT,TAPE3=OUTPUT,TAPE98,TAPE
     X99)
$IBJOB
$IBFTC THII
      DIMENSION J(500),V(500),R(500),X(500),Z(500),Y(500,1),W(150),RESID
     1(150,1),A(20,2),B(20,1),SLOPE(150),XINTER(150),TEMP(150),VO(150),
     2XJSO(150),COLV(10)
      COMMON /CCPOOL/XMIN,XMAX,YMIN,YMAX,CCXMIN,CCXMAX,CCYMIN,CCYMAX
      COMMON /COMIN/OMIN
      COMMON /CCFACT/FACTOR
      EQUIVALENCE (Y,Z)
      REAL J,IN
      FACTOR=1024.
      CCXMIN=.68359375E-01
      CCXMAX=.15332031E+01
      CCYMIN=.78125000E-01
      CCYMAX=.10546875E+01
      IGRAPH=0
      CALL CCBGN
      WRITE (99,1)
    1 FORMAT(28H*WICHNER PLOT - PLAIN PAPER.////)
      OMIN=-2.3025851
      K=0
      READ (2,200) NVCOL
  200 FORMAT(I5)
      IF (NVCOL .GT. 10) NVCOL=10
      ICOL=0
      READ (2,3) (COLV(I),I=1,NVCOL)
    3 FORMAT(6E12.5)
    2 K=K+1
      IF (K .GE. 151) GO TO 4
      READ (2,3) TEMP(K),IN,XMAX,XMIN,Q,DELX
      IF(TEMP(K).EQ.0.0 .AND. IN .EQ. 0.0 .AND. XMAX .EQ. 0.0 .AND. XMIN
     1 .EQ. 0.0) GO TO 4
      WRITE (3,60) TEMP(K),IN,XMAX,XMIN,Q,DELX
   60 FORMAT(1H ,6E12.5)
      READ (2,3) VRMIN,VRMAX,VSMIN,VSMAX,VSCMIN,VSCMAX
      L=0
      IL=(XMAX-XMIN)/DELX+.5
    5 L=L+1
      IF (L.GT. 501) GO TO 6
      READ (2,3) J(L),V(L),R(L)
      IF (V(L) .EQ. 0.0 .AND. J(L) .EQ. 0.0 .AND. R(L) .EQ. 0.0) GO TO 7
      WRITE (3,60)J(L),V(L),R(L)
      GO TO 5
    6 READ (2,3) YREAD,XREAD,RREAD
      IF (XREAD .NE. 0.0 .OR. YREAD .NE. 0.0 .OR. RREAD .NE. 0.0)GO TO 6
    7 L=L-1
      IF (L .GE. 2) GO TO 14
      K=K-1
      GO TO 2
   14 IF (L .GT. 500) L=500
      TEMP(K)=TEMP(K)+273.
      N=0
      DO 8 M=1,L
      J(M)=((J(M)      )/R(M)-IN)/Q
```

```
      IF (J(M) .LE. 0.0) GO TO 8
      N=N+1
      J(N)=ALOG(J(M))
      V(N)=V(M)
      WRITE (3,60)J(N),V(N)
    8 CONTINUE
      WRITE (3,9) TEMP(K)
    9 FORMAT(23H0INITIAL TEMPERATURE = E12.5)
      CALL ORDMAX(J,IO,N)
      LL=N-1
      DO 17 I=1,LL
      TMAX=V(I)
      QMAX=J(I)
      II=I+1
      DO 17 M=II,N
      IF (TMAX .LE. V(M)) GO TO 17
      TMAX=V(M)
      V(M)=V(I)
      V(I)=TMAX
      QMAX=J(M)
      J(M)=J(I)
      J(I)=QMAX
   17 CONTINUE
      IF (IGRAPH .NE. 0) GO TO 18
      IGRAPH=1
      GO TO 19
   18 CALL CCNEXT
   19 CALL CCGRID(IL,6HLABELS,IO)
      WRITE (98,20)
   20 FORMAT(4HLN J)
      CALL CCLTR(0.,574./1024.,1,3)
      WRITE (98,21)
   21 FORMAT(1HV)
      CALL CCLTR(815./1024.,7./1024.,0,3)
      WRITE (98,22) TEMP(K)
   22 FORMAT(13HTEMPERATURE =E13.5)
      CALL CCLTR(1100./1024.,120./1024.,0,2)
      CALL CCPLOT(V,J,N,4HJOIN,7,1)
      M=0
      DO 23 I=1,N
      IF (V(I) .LT. (-5.0)) GO TO 23
      IF (V(I) .GT. 1.0) GO TO 24
      M=M+1
      Z(M)=J(I)
      X(M)=V(I)
   23 CONTINUE
   24 XMIN=-5.0
      XMAX=1.0
      CALL CCNEXT
      CALL CCGRID(6,6HLABELS,IO)
      WRITE (98,20)
      CALL CCLTR(0.,574./1024.,1,3)
      WRITE (98,21)
      CALL CCLTR(815./1024.,7./1024.,0,3)
      WRITE (98,22) TEMP(K)
      CALL CCLTR(1100./1024.,120./1024.,0,2)
      CALL CCPLOT(X,Z,M,4HJOIN,7,1)
      I=0
      DO 25 M=1,N
      IF (V(M) .LT. VRMIN) GO TO 25
      IF (V(M) .GT. VRMAX) GO TO 126
      I=I+1
```

```
      IF (I .GT. 150) GO TO 26
      Y(I,1)=J(M)
      X(I)=V(M)
      W(I)=1.0
   25 CONTINUE
      GO TO 126
   26 I=150
  126 ITEST=1
   27 CALL LSQPOL(X,Y,W,RESID,I,SM,1,A,B,2)
      SIGMA2=FLOAT(I-2)
   28 GO TO (57,57,50,51,52),ITEST
   57 WRITE (3,34)
   34 FORMAT(//8X,1HV,13X,4HLN J,8X,10HLN J CALC.,6X,8HRESIDUAL//)
      GO TO 54
   50 WRITE (3,53)
   53 FORMAT(//3X,12H SQRT(V-VO) ,7X,4HLN J,8X,10HLN J CALC.,6X,8HRESIDU
     1AL//)
      GO TO 54
   51 WRITE (3,55)
   55 FORMAT(//9X,7H1./TEMP,3X,12HLN(JSO/T**2),10X,5HCALC.,7X,8HRESIDUAL
     1//)
      GO TO 54
   52 WRITE (3,56)
   56 FORMAT(//9X,7H1./TEMP,1X,15HLN(JPRIME/T**2),10X,5HCALC.,7X,8HRESID
     1UAL//)
   54 DO 32 M=1,I
      P=B(1,1)+B(2,1)*X(M)
      WRITE (3,33) X(M),Y(M,1),P,RESID(M,1)
   33 FORMAT(1H0,5E15.5)
   32 CONTINUE
      IF (SIGMA2 .LE. 0.)GO TO 35
      SIGMA2=SM/SIGMA2
      DELS=SQRT(SIGMA2*A(2,2))
      DELIN=SQRT(SIGMA2*A(1,1))
      WRITE (3,36)
   36 FORMAT(//10X,1HS,10X,9HINTERCEPT,8X,5HSLOPE,6X,13HDEL INTERCEPT,4X
     1,9HDEL SLOPE)
      WRITE (3,33) SM,B(1,1),B(2,1),DELIN,DELS
      GO TO 37
   35 WRITE (3,38)
   38 FORMAT(//10X,1HS,10X,9HINTERCEPT,8X,5HSLOPE)
      WRITE (3,33) SM,B(1,1),B(2,1)
   37 GO TO (39,40,58,59,80),ITEST
   39 T=11605./B(2,1)
      SLOPE(K)=B(2,1)
      XINTER(K)=B(1,1)
      DELS1=DELS
      DELIN1=DELIN
      DELTT=-(11605.*DELS1)/(SLOPE(K)*(SLOPE(K)+DELS1))
      WRITE (3,41) T,DELTT
   41 FORMAT(//14HOTEMPERATURE =E13.5,10X,13HDELTA TEMP. =E13.5//)
      I=0
      DO 42 L=1,N
      IF (V(L) .LT. VSMIN ) GO TO 42
      IF (V(L) .GT. VSMAX) GO TO 44
      I=I+1
```

```
      IF (I .GT. 150) GO TO 43
      Y(I,1)=J(L)
      X(I)=V(L)
      W(I)=1.0
   42 CONTINUE
      GO TO 44
   43 I=150
   44 ITEST=2
      GO TO 27
   40 XNUM=B(1,1)-XINTER(K)
      DEN=SLOPE(K)-B(2,1)
      DSLOPE=DELS1-DELS
      VO(K)=XNUM/DEN
      DELTVO=(DEN*(DELIN-DELIN1)-XNUM*DSLOPE)/(DEN*(DEN+SLOPE(K)))
      WRITE (3,45) VO(K),DELTVO
   45 FORMAT(//5HOVO =E13.5,10X,10HDELTA VO =E13.5)
      I=0
      DO 46 L=1,N
      IF (V(L) .LT. VO(K) .OR. V(L) .LT. VSCMIN) GO TO 46
      IF (V(L) .GT. VSCMAX) GO TO 146
      I=I+1
      IF (I .GT. 150) GO TO 147
      X(I)=SQRT(V(L)-VO(K))
      Z(I)=J(L)
      Y(I,1)=Z(I)
      W(I)=1.0
   46 CONTINUE
      GO TO 146
  147 I=150
  146 IMAX=X(I)+1.5
      XMAX=FLOAT(IMAX)+.000001
      XMIN=0.
      CALL ORDMAX(Z,IO,I)
      CALL CCNEXT
      CALL CCGRID(10,6HLABELS,IO)
      WRITE (98,47)
   47 FORMAT(5HLN JS)
      CALL CCLTR(-7./1024.,574./1024.,1,3)
      WRITE (98,48)
   48 FORMAT(10HSQRT(V-VO))
      CALL CCLTR(802./1024.,0.,0,3)
      WRITE (98,22) TEMP(K)
      CALL CCLTR(1100./1024.,120./1024.,0,2)
      CALL CCPLOT(X,Z,I,4HJOIN,6,1)
      ITEST=3
      GO TO 27
   58 XJSO(K)=EXP(B(1,1))
      WRITE (3,61) XJSO(K)
   61 FORMAT(6HOJSO =E12.5//)
      GO TO 2
    4 K=K-1
      IF (K .LT. 2) RETURN
      DO 63 L=1,K
      Y(L,1)=ALOG(XJSO(L)/TEMP(L)**2)
      X(L)=1./TEMP(L)
      W(L)=1.0
   63 CONTINUE
      ITEST=4
      I=K
      GO TO 27
   59 CALL CCNEXT
      LL=K-1
```

```
      DO 67 L=1,LL
      TMAX=X(L)
      QMAX=Y(L,1)
      DO 68 M=L,K
      IF (TMAX .LE. X(M)) GO TO 68
      TMAX=X(M)
      X(M)=X(L)
      X(L)=TMAX
      QMAX=Y(M,1)
      Y(M,1)=Y(L,1)
      Y(L,1)=QMAX
   68 CONTINUE
      Z(L)=Y(L,1)
   67 CONTINUE
      Z(K)=Y(K,1)
      XMIN=0.0
      XMAX=.00125
      CALL ORDMAX(Z,IO,K)
      CALL CCGRID(10,6HLABELS,IO)
      PHIE=-B(2,1)/11605.
      WRITE (3,64) PHIE
   64 FORMAT(16HOPHI (EMITTER) =E12.5//)
      WRITE (98,65)
   65 FORMAT(12HLN(JSO/T**2))
      CALL CCLTR(-7./1024.,562./1024.,1,3)
      WRITE (98,66)
   66 FORMAT(3H1/T)
      CALL CCLTR(815./1024.,0.,0,3)
      CALL CCPLOT(X,Z,K,4HJOIN,6,1)
  201 ICOL=ICOL+1
      VCOL=COLV(ICOL)
      DO 70 L=1,K
      Y(L,1)=ALOG(EXP(XINTER(L)+SLOPE(L)*VCOL)/TEMP(L)**2)
      X(L)=1./TEMP(L)
      W(L)=1.0
   70 CONTINUE
      ITEST=5
      GO TO 27
   80 CALL CCNEXT
      DO 74 L=1,LL
      TMAX=X(L)
      QMAX=Y(L,1)
      DO 75 M=L,K
      IF (TMAX .LE. X(M))GO TO 75
      TMAX=X(M)
      X(M)=X(L)
      X(L)=TMAX
      QMAX=Y(M,1)
      Y(M,1)=Y(L,1)
      Y(L,1)=QMAX
   75 CONTINUE
      Z(L)=Y(L,1)
   74 CONTINUE
      Z(K)=Y(K,1)
      CALL ORDMAX(Z,IO,K)
      PHIE=-B(2,1)/11605.
```

```
      WRITE (3,71) VCOL,PHIE
   71 FORMAT(14HOV COLLECTOR =E12.5,18H PHI (COLLECTOR) =E12.5//)
      CALL CCGRID(10,6HLABELS,IO)
      WRITE (98,72)
   72 FORMAT(15HLN(JPRIME/T**2))
      CALL CCLTR(-7./1024.,558./1024.,1,3)
      WRITE (98,66)
      CALL CCLTR(815./1024.,0.,0,3)
      WRITE (98,73) VCOL
   73 FORMAT(6HVCOL =E13.5)
      CALL CCLTR(1300./1024.,120./1024.,0,2)
      CALL CCPLOT(X,Z,K,4HJOIN,7,1)
      IF (ICOL .NE. NVCOL) GO TO 201
      CALL CCEND
      RETURN
      END
```

```
      SUBROUTINE ORDMAX(J,IO,N)
      DIMENSION J(1)
      COMMON /CCPOOL/XMIN,XMAX,YMIN,YMAX,CCXMIN,CCXMAX,CCYMIN,CCYMAX
      COMMON /COMIN/OMIN
      REAL J
      VMAX=J(1)
      VMIN=J(1)
      DO 10 I=2,N
      VMAX=AMAX1(VMAX,J(I))
      VMIN=AMIN1(VMIN,J(I))
   10 CONTINUE
      CONST=1.
      IMAX=ABS(VMAX/OMIN)
      IF (VMAX .LT. 0.)GO TO 12
      CONST=-1.
      IMAX=IMAX+1
   12 YMAX=FLOAT(IMAX)*OMIN*CONST
      CONST=-1.
      IMAX=ABS(VMIN/OMIN)
      IF (VMIN .GT. 0.)GO TO 13
      IMAX=IMAX+1
      CONST=1.
   13 YMIN=FLOAT(IMAX)*OMIN*CONST
   15 IO=(YMAX-YMIN)/(-OMIN)+.5
      RETURN
      END
```

```
$IBFTC LSQPOL
C       LEAST SQUARE POLYNOMIAL FIT                                     ANE20601
C                                                                       ANE20602
        SUBROUTINE LSQPOL(X,Y,W,RESID,N,SUM,L,A,B,M)                    ANE20603
C                                                                       ANE20604
        DIMENSION X(150),Y(150,1),RESID(150,1),A(20,8),B(20,8),C(150,8)
       1,SUM(1),W(150)
        COMMON /LSP/ C
C                                                                       ANE20608
   10 DO 20 I=1,N                                                       ANE20609
   20 C(I,1)=1.0                                                        ANE20610
   30 DO 50 J=2,M                                                       ANE20611
   40 DO 50 I=1,N                                                       ANE20612
   50 C(I,J)=C(I,J-1)*X(I)                                              ANE20613
   60 DO 100 I=1,M                                                      ANE20614
   70 DO 100 J=1,M                                                      ANE20615
   80 A(I,J)=0.0                                                        ANE20616
   90 DO 100 K=1,N                                                      ANE20617
  100 A(I,J)=A(I,J)+C(K,I)*C(K,J)*W(K)                                  ANE20618
  105 DO 150 J=1,L                                                      ANE20619
  110 DO 150 I=1,M                                                      ANE20620
  120 B(I,J)=0.0                                                        ANE20621
  130 DO 150 K=1,N                                                      ANE20622
  150 B(I,J)=B(I,J)+C(K,I)*Y(K,J)*W(K)                                  ANE20623
 170  CALL MATINV (A,M,B,L,DETERM)
  180 DO 205 J=1,L                                                      ANE20625
  185 SUM(J)=0.0                                                        ANE20626
  192 DO 195 K=1,M                                                      ANE20627
  195 C(K,1)=B(K,J)                                                     ANE20628
  198 DO 205 I=1,N                                                      ANE20629
  200 RESID(I,J)=POLYE1(X(I),M,C(1,1))-Y(I,J)
  205 SUM(J)=SUM(J)+RESID(I,J)**2*W(I)                                  ANE20631
  210 RETURN                                                            ANE20632
 220  END
$IBFTC MATINV  LIST,REF
C       MATRIX INVERSION WITH ACCOMPANYING SOLUTION OF LINEAR EQUATIONS ANE40201
C                                                                       E4020002
        SUBROUTINE MATINV(A,N,B,M,DETERM)                               E4020003
C                                                                       E4020004
        DIMENSION IPIVOT(20), A(20,20), B(20,1), INDEX(20,2), PIVOT(20) E4020005
        COMMON /LSP/ PIVOT,IPIVOT,INDEX
        EQUIVALENCE (IROW,JROW), (ICOLUM,JCOLUM), (AMAX, T, SWAP)       E4020007
C                                                                       E4020008
C       INITIALIZATION                                                  E4020009
C                                                                       E4020010
   10 DETERM=1.0                                                        E4020011
   15 DO 20 J=1,N                                                       E4020012
   20 IPIVOT(J)=0                                                       E4020013
   30 DO 550 I=1,N                                                      E4020014
C                                                                       E4020015
C       SEARCH FOR PIVOT ELEMENT                                        E4020016
C                                                                       E4020017
   40 AMAX=0.0                                                          E4020018
   45 DO 105 J=1,N                                                      E4020019
   50 IF (IPIVOT(J)-1) 60, 105, 60                                      E4020020
   60 DO 100 K=1,N                                                      E4020021
```

```
   70 IF (IPIVOT(K)-1) 80, 100, 740                                    F4020022
   80 IF (ABS(AMAX)-ABS(A(J,K))) 85, 100, 100
   85 IROW=J                                                           F4020024
   90 ICOLUM=K                                                         F4020025
   95 AMAX=A(J,K)                                                      F4020026
  100 CONTINUE                                                         F4020027
  105 CONTINUE                                                         F4020028
  110 IPIVOT(ICOLUM)=IPIVOT(ICOLUM)+1                                  F4020029
C                                                                      F4020030
C     INTERCHANGE ROWS TO PUT PIVOT ELEMENT ON DIAGONAL                F4020031
C                                                                      F4020032
  130 IF (IROW-ICOLUM) 140, 260, 140                                   F4020033
  140 DETERM=-DETERM                                                   F4020034
  150 DO 200 L=1,N                                                     F4020035
  160 SWAP=A(IROW,L)                                                   F4020036
  170 A(IROW,L)=A(ICOLUM,L)                                            F4020037
  200 A(ICOLUM,L)=SWAP                                                 F4020038
  205 IF(M) 260, 260, 210                                              F4020039
  210 DO 250 L=1, M                                                    F4020040
  220 SWAP=B(IROW,L)                                                   F4020041
  230 B(IROW,L)=B(ICOLUM,L)                                            F4020042
  250 B(ICOLUM,L)=SWAP                                                 F4020043
  260 INDEX(I,1)=IROW                                                  F4020044
  270 INDEX(I,2)=ICOLUM                                                F4020045
  310 PIVOT(I)=A(ICOLUM,ICOLUM)                                        F4020046
  320 DETERM=DETERM*PIVOT(I)                                           F4020047
C                                                                      F4020048
C     DIVIDE PIVOT ROW BY PIVOT ELEMENT                                F4020049
C                                                                      F4020050
  330 A(ICOLUM,ICOLUM)=1.0                                             F4020051
  340 DO 350 L=1,N                                                     F4020052
  350 A(ICOLUM,L)=A(ICOLUM,L)/PIVOT(I)                                 F4020053
  355 IF(M) 380, 380, 360                                              F4020054
  360 DO 370 L=1,M                                                     F4020055
  370 B(ICOLUM,L)=B(ICOLUM,L)/PIVOT(I)                                 F4020056
C                                                                      F4020057
C     REDUCE NON-PIVOT ROWS                                            F4020058
C                                                                      F4020059
  380 DO 550 L1=1,N                                                    F4020060
  390 IF(L1-ICOLUM) 400, 550, 400                                      F4020061
  400 T=A(L1,ICOLUM)                                                   F4020062
  420 A(L1,ICOLUM)=0.0                                                 F4020063
  430 DO 450 L=1,N                                                     F4020064
  450 A(L1,L)=A(L1,L)-A(ICOLUM,L)*T                                    F4020065
  455 IF(M) 550, 550, 460                                              F4020066
  460 DO 500 L=1,M                                                     F4020067
  500 B(L1,L)=B(L1,L)-B(ICOLUM,L)*T                                    F4020068
  550 CONTINUE                                                         F4020069
C                                                                      F4020070
C     INTERCHANGE COLUMNS                                              F4020071
C                                                                      F4020072
  600 DO 710 I=1,N                                                     F4020073
  610 L=N+1-I                                                          F4020074
  620 IF (INDEX(L,1)-INDEX(L,2)) 630, 710, 630                         F4020075
  630 JROW=INDEX(L,1)                                                  F4020076
  640 JCOLUM=INDEX(L,2)                                                F4020077
  650 DO 705 K=1,N                                                     F4020078
  660 SWAP=A(K,JROW)                                                   F4020079
  670 A(K,JROW)=A(K,JCOLUM)                                            F4020080
  700 A(K,JCOLUM)=SWAP                                                 F4020081
  705 CONTINUE                                                         F4020082
  710 CONTINUE                                                         F4020083
```

```
  740 RETURN
  750 END                                                    E4020084
$IBFTC POLY                                                  E4020085
      FUNCTION POLYE1(X,M,C)
      DIMENSION C(50,1)
      S=C(M,1)
      N=M-1
      DO 1 I=1,N
      K=M-I
      S=S*X+C(K,1)
    1 CONTINUE
      POLYE1=S
      RETURN
      END
```

ERROR ANALYSIS

3. As described above, the data in each part of Therm II was fitted to a straight line by means of a least squares analysis. The method of least squares is outlined below:

Given a set of N experimental values of an independent variable, x, with a corresponding set of values of a dependent variable, y, we assume that the observed points, (x_i, y_i) approximate a straight line of the form,

$$y = mx + b \tag{D.3}$$

As an example, for the Richardson plot, $y = \ln \frac{J_{so}}{T^2}$, $x = \frac{1}{T}$, $m = \frac{-e\phi}{k}$ and $b = \ln A_r$.

The sum, S, of the squares of the residuals, $[y(x_i) - y_i]$, is

$$S = \sum_{i=1}^{N} [y(x_i) - y_i]^2 \tag{D.4}$$

where each point, (x_i, y_i) is assumed to have equal weight. The object of the least squares analysis is to minimize S. The values of m and b which minimize S are

$$m = \frac{N\Sigma(x_i y_i) - \Sigma x_i \Sigma y_i}{N\Sigma x_i^2 - (\Sigma x_i)^2} \tag{D.5}$$

and

$$b = \frac{\Sigma x_i^2 \, \Sigma y_i - \Sigma x_i \, \Sigma(x_i y_i)}{N\Sigma x_i^2 - (\Sigma x_i)^2} \tag{D.6}$$

Now assuming that all of the errors in the measurements are lumped in the y_i's, the standard error, σ, for the parent distribution is

$$\sigma = \left[\frac{\Sigma(y(x_i) - y_i)^2}{N - 2} \right]^{1/2} \tag{D.7}$$

We use N-2 in the denominator because the number of degrees of freedom is two less than N as a result of the two arbitrary parameters, m and b.

In addition, the standard errors of m and b are given by

$$\sigma_m = \left(\frac{N}{N\Sigma x_i^2 - (\Sigma x_i)^2} \right)^{1/2} \sigma \tag{D.8}$$

and

$$\sigma_b = \left(\frac{\Sigma x_i^2}{N\Sigma x_i - (\Sigma x_i)^2} \right)^{1/2} \sigma \tag{D.9}$$

The assumption that all of the error can be assigned to the y_i values will be shown to be a reasonable one.

In calculating V_o and J_{so}, the x_i's are the measured voltages, V, and the y_i's are the measured currents. The instrumentation amplifiers and voltmeter were calibrated and found to be accurate to ± .02%. The error in the value of V is therefore on the order of the uncertainty of the instrumentation. However, the uncertainty in the current can be much larger. The value of the current is determined by the voltage drop across the collector resistor, V_{cr}, which is known to ±.05%. But by far the largest uncertainty in J is that associated with the temperature. Typically, for an emitter at 2000°K with ϕ = 5 ev, a change in temperature of 1°K results in a change of approximately 2% in J, so that reading the emitter temperature to ± 5°K results in an uncertainty of 10% in J.

Another uncertainty in the value of J is that associated with the area of the collector. V_{cr} divided by the value of the collector resistor yields the current, which must then be divided by the area of the collector to obtain J, the current density. However, because of the gap between the collector and guard ring, the actual area over which the current was collected was known to only ±16%. Thus, for the least squares analysis for finding the equations of the retarded, saturated, and Schottky lines, the assumption that the error in x_i can be neglected is justified.

In the Richardson and Shelton plots, where x is equal to 1/T, the above assumption is still valid. The uncertainty of ±5°K over the entire temperature range corresponds to less than 0.5% whereas the uncertainty associated with J_{so} as shown above can be as high as 25%, which includes the uncertainty associated with the temperature and that associated with the area.

This large uncertainty in J_{so}, as a result of the uncertainty of the collector area, manifests itself as an uncertainty in the value of A_r, but has little effect upon the values obtained for Φ. An error in T, however, affects the value obtained for Φ. Typically, for an emitter work function of 5 ev, at a temperature of 2000°K, an error of 5°K results in an error of 0.25% in Φ.

The above discussion has considered only the random errors involved in the experiments. Systematic errors in these experiments are considered to be minor. The major systematic error in the experiments is associated with the determination of the true emitter temperature. Although the optical pyrometer was calibrated with the viewing port, it is possible that with the high emitter temperatures reached, sufficient material

was evaporated onto the viewing port to decrease the transmission of light. This would result in an underestimate of the temperature. This underestimate would be less than 2% since the power input to the emitter was monitored and no perceptible increase was necessary at the end of the experiments to bring the emitter to the same temperature as was needed at the beginning. All other systematic errors, such as instrumentation drift or offset, were found to be negligible.

In this error analysis, mention must be made of an error to which no numerical value can be given. This error is associated with the assumption that the surface atoms of the monocrystalline emitters have the same arrangement as the interior atoms. Although the Laué x-ray photographs indicate a distortion-free crystal, the x-rays penetrate far beyond the first couple of atomic layers. It is precisely these first layers, however, which greatly influence the work function. In the case of the (0001) and $(10\bar{1}1)$ orientations it is felt that the surfaces were indeed representative of the interior atoms arrangements. However, because of the microscopic surface distortion observed on the $(10\bar{1}0)$ emitter, and in view of the questions raised in Section V, it appears that the surface arrangement of atoms may not have been exactly that of the interior. Just how much distortion exists and how much $\Phi_{(10\bar{1}0)}$ is affected eludes calculation.

APPENDIX E

DATA ACQUISITION SYSTEM

The following considerations were taken into account in designing the data acquisition system:

1. The instrumentation used for measuring the diode current must have a high input impedance to avoid loading errors,
2. The collector and guard-ring must be kept at equal potential throughout the entire voltage swing of the collector,
3. The entire I-V curve must be obtained within a few minutes to avoid changes as a result of temperature or instrumentation drift. Similarly, when the emitter is flashed to clean the surface, the data must also be obtained rapidly, before any change in the work function occurs due to adsorption of gases on the emitter surface,
4. Current-voltage data must be in a form compatible with the Resist and Therm II codes, used with the CDC 6600 computer to analyze the data.

Figure E.1 represents a simplified schematic diagram of the diode circuit. V is the voltage across the diode, V_{cr} is the voltage drop across the collector resistor and V_{gc} is the voltage between the guard-ring and collector. The I-V curve of the diode was obtained by varying the power supply between -5 volts and +65 volts and measuring the collector resistor voltage drop, V_{cr}, at any given value of V.

Figure E.2 represents a more detailed view of the diode circuit. The X1 and X10 amplifiers are Philbrick SP2A operational amplifiers, selected because of their high input impedance, 10^{12} ohms. The guard-ring amplifier and its power supply, shown schematically in Figs. E.3 and

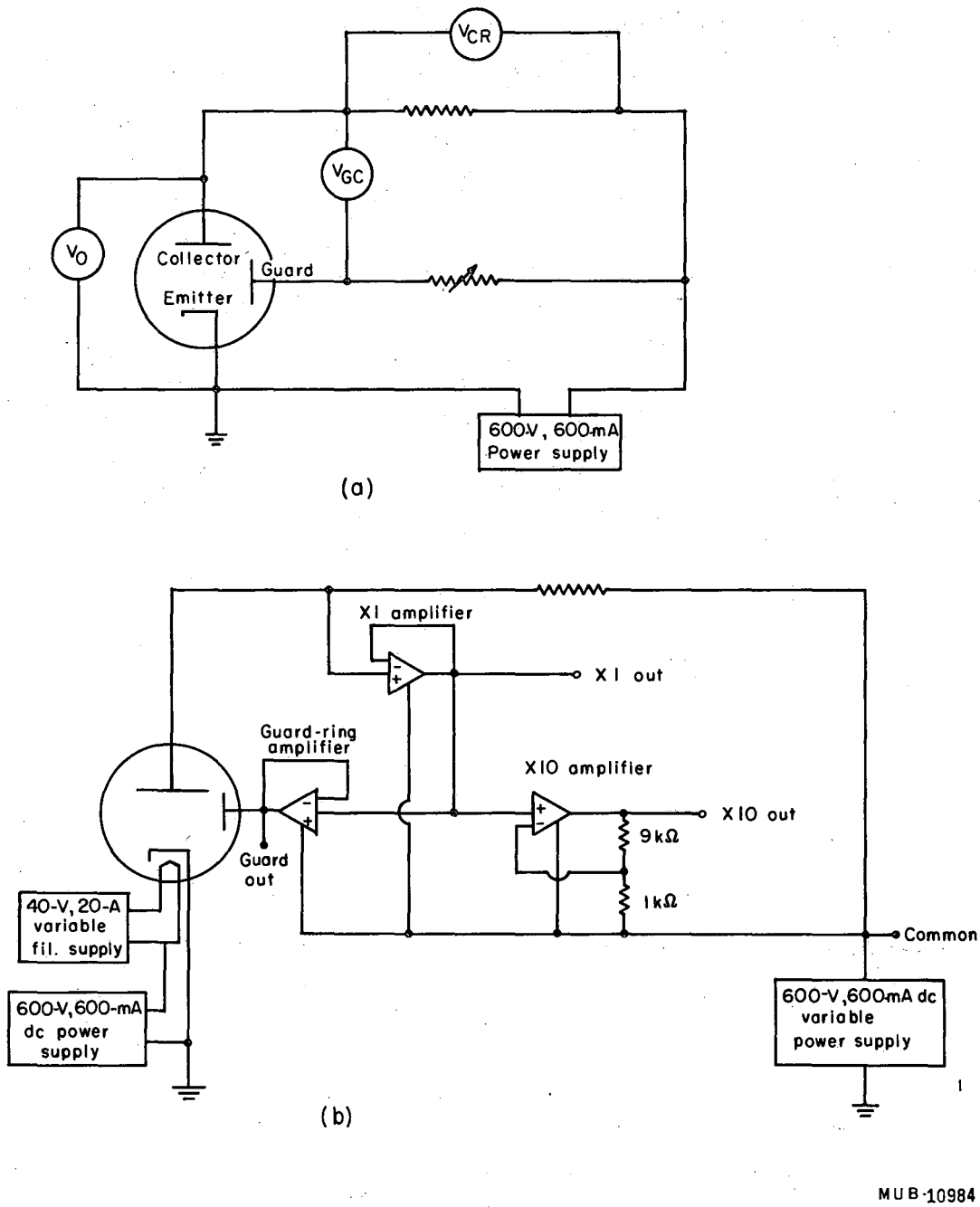
VCR
VGC
VO
Collector
Guard
Emitter
600-V, 600-mA
Power supply
(a)
X1 amplifier
X1 out
Guard-ring
amplifier
X10 amplifier
X10 out
9kΩ
1kΩ
Guard
out
40-V, 20-A
variable
fil. supply
600-V, 600-mA
dc power
supply
Common
600-V, 600-mA dc
variable
power supply
(b)
MUB-10984

Fig. E.1

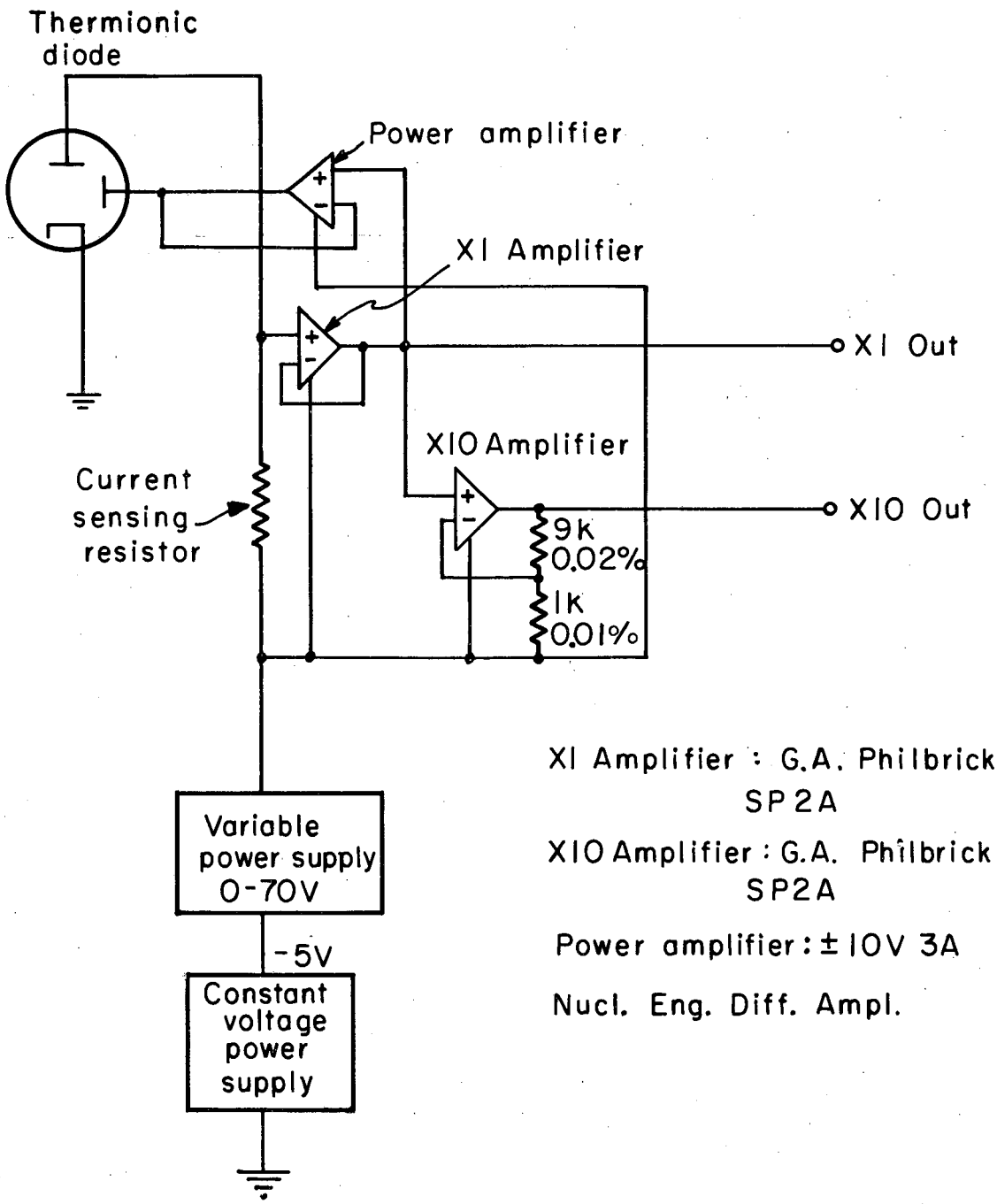

Fig. E.2

MUB 12042

E.4 , were designed to maintain the collector-guard voltage, V_{gc} at or near zero volts, regardless of the voltage across the diode, V, and regardless of the voltage drop across the collector resistor, V_{cr}. This amplifier was able to maintain V_{gc} to less than 100 microvolts, which is the sensitivity of the voltmeter used in the experiments. The voltmeter, a Dana Model 5603 digital voltmeter, read V by measuring between the X1 output and ground. It read V_{cr} by measuring between X10 out and common. This gave a value for V_{cr} that was 10 times the true V_{cr}, but this was necessary to utilize the Dana to its full sensitivity. (Because the programmable power supply could not easily compensate for V_{cr} (true) > 1 volt, V_{cr} was kept between 0.1 and 1 volt by selecting the proper collector resistor.) This factor of 10 was compensated for in the input information to the computer by increasing the collector resistor values by a factor of 10. The above met the first two requirements of the data acquisition system.

In order to meet requirements 3 and 4, an electronic logic system was designed and built so that pre-selected voltages would be applied to the diode, the current at each voltage measured, and this information put on perforated paper tape. The Dana digital voltmeter, which was used to measure both current and voltage data, fed binary coded information into a CMC Model 403A adapter which fed a Tally P-120 paper tape perforator. The perforated tape was then converted into IBM data cards of the proper format by means of an IBM Model 46 card punch. Figure E. 5 shows a flow sheet for the logical sequence of events in obtaining a current-voltage curve, consisting of 70 data points. The voltage across the diode was set by means of a programmable Regatron 235 AMK power supply. The voltage output from this supply was determined

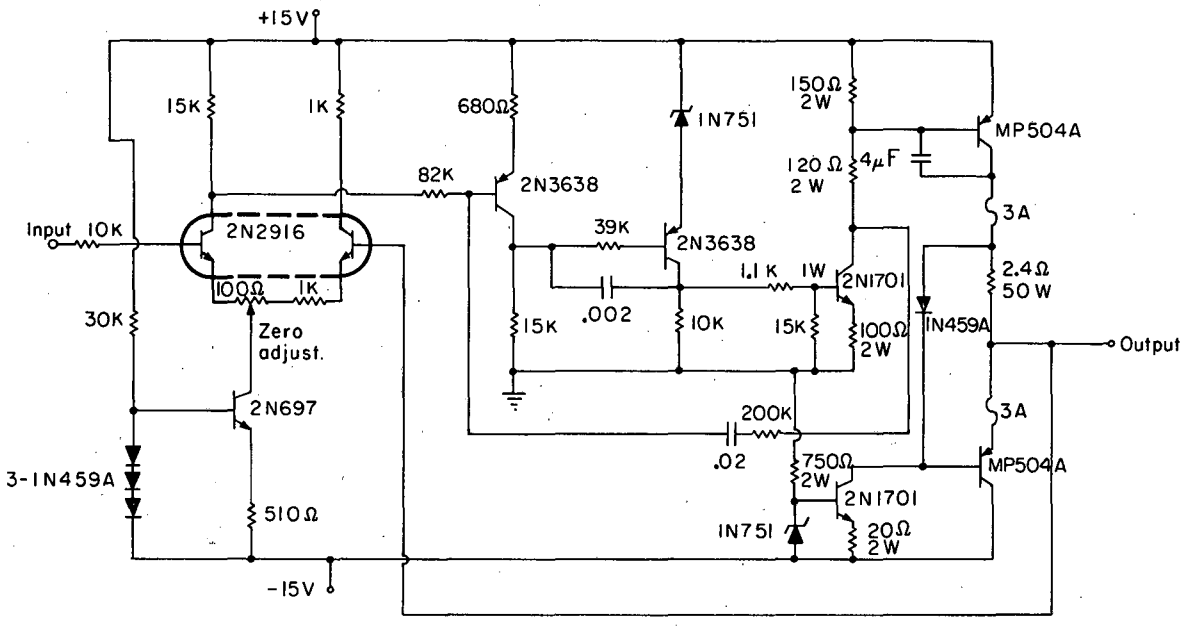

All resistors 1/4 W 5% unless otherwise specified

MUB-9480

Fig. E.3

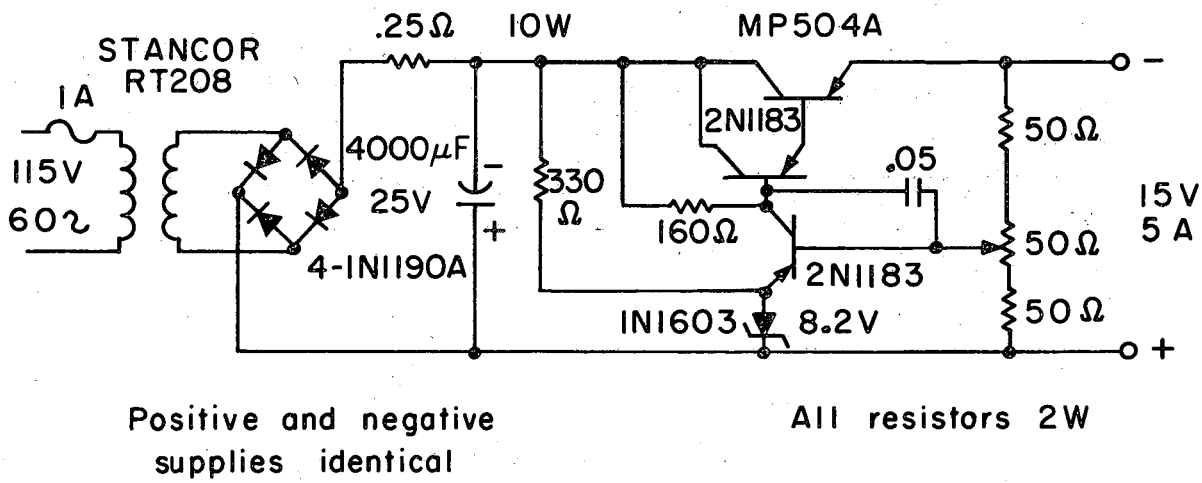
STANCOR
RT208
1A
115V
60~
.25Ω
10W
4000μF
25V
4-1N1190A
330
Ω
160Ω
MP504A
2N1183
.05
2N1183
1N1603
8.2V
50Ω
50Ω
50Ω
15V
5 A
Positive and negative
supplies identical
All resistors 2W
MUB-9479

Fig. E.4

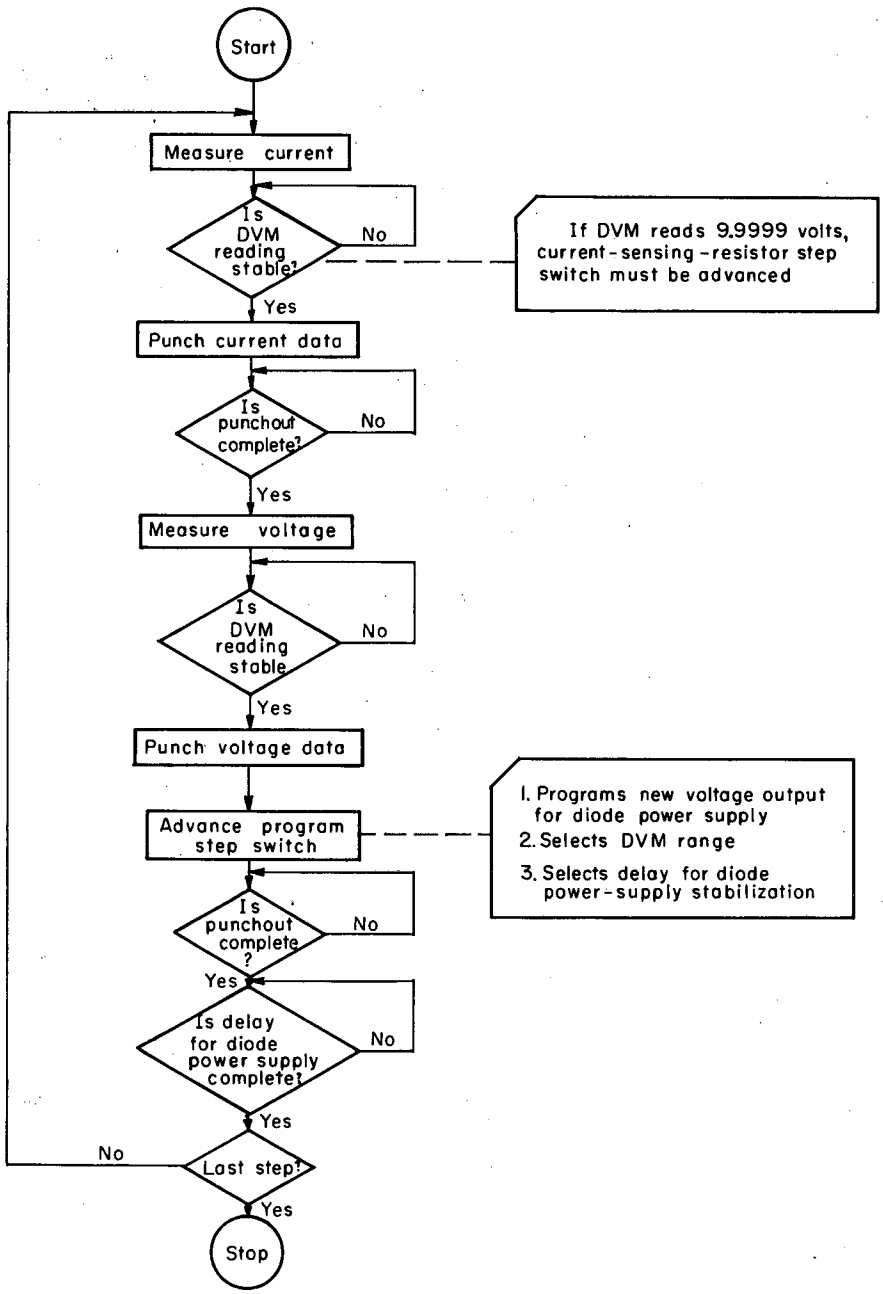

MUB-12047

Fig. E.5

by selecting one of a series of 70 programming resistors, each resistor value determining a given output voltage. The schematic diagrams of the logic system are available as LRL Print numbers 10V402-1 through 10V402-8.

Figure E.6 shows an overall view of the experimental set-up.

ZN-5575

Fig. E.6

REFERENCES

1. John M. Houston, State of the Art Survy of Thermionic Conversion for Electrical Space Power, General Electric Research and Development Center, Schenectady, New York Report No. 65-RL-(4024E), August 1965.

2. F. J. Kycsko and H. L. Traiger, Development of a Lightweight Gasoline Fueled Thermionic Engine, Thermionic Conversion Specialist Conference, Gatlinburg, Tenn., October 7-9, 1963, p. 362.

3. Wayne B. Nottingham, Handbuch Der Physik, Vol. XXI, Electron Emission (Springer-Verlag, Berlin, 1956) Ch. 1.

4. Wayne B. Nottingham, Emitter Materials for High Temperature Energy Conversion, Proceedings of the International Symposium on High Temperature Technology, September 8-11, 1963.

5. Ned S. Rasor, Atomics International Report No. AI-6799, Nov. 1961.

6. William H. Gust, Emission Characteristics of Tantalum, Tungsten, Rhenium and Iridium in Plasma Diodes, UCRL-6809 Rev. 1, (April 1962).

7. S. S. Kitrilakis, et al., Annual Technical Summary Report for the Thermionic Emitter Materials Research Program, TEECO Report No. 2-63, Thermo Electron Engineering Corp., Walyham, Mass.

8. R. Smoluchowski, Phys. Rev. 60, 661 (1941).

9. E. N. Carabateas, R. Stickney and T. Aponick, Basic Studies of Cerium Thermionic Converters, Report to the National Science Foundation, Project Number DSR 8955, Energy Conversion Laboratory, Mass. Inst. of Tech., Cambridge, Mass.

10. G. J. Daly and J. L. Gumnick, Field Emission Studies of Cs Migration on Re, Report on 22nd Annual Conference on Physical Electronics, Mass. Inst. of Tech., March 21-23, 1962, pg. 164.

11. M. N. Huberman and R. A. Holzl, Uniform Work Function Emitter Studies, Thermionic Conversion Specialist Conference, Gatlinburg, Tenn., Oct. 7-9, 1963 p. 179.

12. Ira Weissman, Grain-Oriented Thoriated Tungsten Emitters for Thermionic Energy Converters, Thermionic Conversion Specialist Conference, Cleveland, Ohio, October 26-28, 1964, p.39.

13. T. Allean, et al., The Study of the Work Function Distribution on Chemical Vapour-Deposited Tungsten, Thermionic Conversion Specialist Conference, San Diego, Calif., Oct. 25-27, 1965, p. 367.

14. Albert J. van der Ziel, Solid State Physical Electronics (Prentice-Hall, Inc., New York, 1957) p. 104.

15. Haywood Shelton, Phys. Rev. 107, 1553 (1957).

16. E. Wigner and J. Bardeen, Phys. Rev. 48, 84 (1935).

17. C. Herring and M. H. Nichols, Rev. Mod. Phys. 21, 185 (1949).

18. J. Bardeen, Phys. Rev. 49, 633 (1936).

19. T. Batzer, UCID;4548, Rev. IV, Lawrence Radiation Laboratory, Livermore, Calif., Jan. 1966.

20. Index to the X-Ray Powder Data File, ASTM Spec. Tech. Publ. 48-L (1962).

21. E. M. Savitskii and M. A. Tylkina, Phase Diagrams of Re with Transition Metals, in Rhenium, B. W. Gonser, Ed. (Elselvier Pub.Co.,New York, 1962).

22. A. G. Knapton, Journal of the Less-Common Metals, 1, 480 (1959).

23. W. J. McG. Tegart, The Electrolytic and Chemical Polishing of Metals in Research and Industry (Pergamon Press, New York, 1959) p. 102.

24. C. A. Hampel, Ed., Rare Metals Handbook, 2nd Edition (Reinhold Pub. Corp., London, 1961) p. 170.

25. R. Benson, UCLRL, Private Communication.

26. J. L. Gumnick and G. J. Daly, Bull. Am. Phys. Soc. 6, 421 (1961).

27. J. Anderson, et al., J. Appl. Phys. 34, 2260 (1963).

28. A. L. Hyland, AD-406926 (1963).

29. V. C. Wilson and J. Lawrence, Advanced Energy Conversion, 4, 195 (1964).

30. Yu. K. Gus'kov, et al., Izvestiya Akad. Nauk SSSR, Servia Fiz. 28, 1537 (1964).

31. W. Weierhausen, Annalen Der Physik, 15: 1-2 (1965).

32. R. G. Wilson, NASA-CR-54679.

33. H. F. Webster, The Thermionic Converter with Uniform Work Function Electrodes, Report No. 65-RL-3837E, General Electric Research Laboratory, Jan. 1965.

34. N. S. Rasor and C. Warner, J. Appl. Phys. 35, 2589 (1964).

35. H. F. Webster, Bull. Am. Phys. Soc.[2] 6, 343 (1961); J. Appl. Phys. 32, 1802 (1961); Cited by J. M. Houston and H. F. Webster, Adv. in Electronics and Electron Physics 17, 125 (1963).

36. Handbook of Chemistry and Physics, 42nd Ed. (The Chemical Rubber Publishing Co., Cleveland, Ohio, 1960) p. 2558.

37. H. Mark and N. T. Olson, Experiments in Modern Physics (McGraw-Hill Book Co., New York, 1966) p. 219.

FIGURE CAPTIONS

Fig. II.1 (a) Ideal curve of electron emission density, J, vs applied collector voltage, V, for a vacuum diode having an emitter with work function and a collector with work function Φ_c such that $\Phi' > \Phi_c$. (b) Motive diagrams corresponding to each of the regions in (a).

Fig. II.2 Side view of HCP Re lattice, where a and c are the lattice parameters. Crosses indicate the position of atoms in the lattice. (1) and (2) refer to the number of atoms within the same radius, r. (0001), $(10\bar{1}0)$ and $(10\bar{1}1)$ correspond to the planes in the lattice. The plane of the page is $(11\bar{2}0)$.

Fig. III.1 Thermionic diode assembly, mounted in vacuum chamber.

Fig. III.2 Cross-section of diode test stand.

Fig. III.3 Test stand used for brazing.

Fig. III.4 Section of Re-Ta discs brazed with Nb foil which was not outgassed.

Fig. III.5 Section of successful Re-Nb-Ta braze.

Fig. III.6 Schematic diagram of vacuum system.

Fig. IV.1 Calibration curve used to determine true emitter temperature.

Fig. V.1 Typical $\ln$ J-V curve ($(10\bar{1}0)$ Re, Run No. 65, T = 2177°K) (J in amps/cm^2, V in volts).

Fig. V.2 Retarded region of Run No. 65 (J in amps/cm^2, V in volts).

Fig. V.3 Typical resistive leakage-current region of I-V data.

Fig. V.4 Retarded region, corrected for resistive leakage current (J in amps/cm^2, V in volts).

Fig. V.5 $\ln$ J vs V for a typical "(0001)" run. A is the retarded region slope, B is the transition region, C is the saturated current density, J_{so}. (Run No. 108, T = 2093°K).

Fig. V.6 Microscopic view of surface of $(10\bar{1}0)$ Re emitter, after the experiments. (Original magnification: 400×, enlarged to 750×.)

Fig. V.7 Schottky plot for Run No. 65 (J_s in amps/cm^2, V in volts).

Fig. V.8 Richardson plot for polycrystalline Re emitter (J_{so} in amps/cm^2, T in °K).

Fig. V.9 Richardson plot for $(10\bar{1}1)$ Re emitter (J_{so} in amps/cm^2, T in °K).

Fig. V.10 Richardson plot for $(10\bar{1}0)$ Re emitter (J_{so} in amps/cm^2, T in °K).

Fig. V.11 Calculated Richardson plot for (0001) orientation. This was obtained from the (0001) data using the assumption of a two-patch surface.

Fig. B.1 Laue x-ray picture of $(10\bar{1}0)$ Re.

Fig. B.2 Laue x-ray picture of $(10\bar{1}1)$ Re.

Fig. B.3 Laue x-ray picture of (0001) Re.

Fig. C.1 ℓn I-V curve for a two-patch emitter. Curves 1 and 2 represent the ℓn I-V curves for each patch.

Fig. E.1 (a) Simplified schematic of diode test circuit. (b) Block diagram of diode test circuit.

Fig. E.2 Schematic of diode test circuit. The constant voltage power supply provides a bias of -5 volts. This results in a variable range of -5 to +65 volts across the diode.

Fig. E.3 Guard-ring amplifier.

Fig. E.4 Power supply for guard-ring amplifier.

Fig. E.5 Flow sheet for automatic data acquisition system.

Fig. E.6 View of the electronic equipment and vacuum system.

This report was prepared as an account of Government sponsored work. Neither the United States, nor the Commission, nor any person acting on behalf of the Commission:

A. Makes any warranty or representation, expressed or implied, with respect to the accuracy, completeness, or usefulness of the information contained in this report, or that the use of any information, apparatus, method, or process disclosed in this report may not infringe privately owned rights; or

B. Assumes any liabilities with respect to the use of, or for damages resulting from the use of any information, apparatus, method, or process disclosed in this report.

As used in the above, "person acting on behalf of the Commission" includes any employee or contractor of the Commission, or employee of such contractor, to the extent that such employee or contractor of the Commission, or employee of such contractor prepares, disseminates, or provides access to, any information pursuant to his employment or contract with the Commission, or his employment with such contractor.